



Scattering and absorption properties of near-surface aerosol over Gangetic–Himalayan region: the role of boundary-layer dynamics and long-range transport

U. C. Dumka¹, D. G. Kaskaoutis², M. K. Srivastava³, and P. C. S. Devara⁴

¹Aryabhata Research Institute of Observational Sciences, Nainital, India

²Department of Physics, School of Natural Sciences, Shiv Nadar University, Tehsil Dadri, India

³Department of Geophysics, Banaras Hindu University, Varanasi, India

⁴Amity Centre for Ocean-Atmospheric Science and Technology (ACOAST), Amity University Haryana, Gurgaon (Manesar), India

Correspondence to: U. C. Dumka (dumka@aries.res.in; ucdumka@gmail.com)

Received: 27 June 2014 – Published in Atmos. Chem. Phys. Discuss.: 18 August 2014

Revised: 16 January 2015 – Accepted: 16 January 2015 – Published: 13 February 2015

Abstract. Light scattering and absorption properties of atmospheric aerosols are of vital importance for evaluating their types, sources and radiative forcing. This is of particular interest over the Gangetic–Himalayan (GH) region due to uplift of aerosol from the plains to the Himalayan range, causing serious effects on atmospheric heating, glaciology and monsoon circulation. In this respect, the Ganges Valley Aerosol Experiment (GVAX) was initiated in Nainital from June 2011 to March 2012 with the aim of examining the aerosol properties, source regions, uplift mechanisms and aerosol–radiation–cloud interactions. The present study examines the temporal (diurnal, monthly, seasonal) evolution of scattering (σ_{sp}) and absorption (σ_{ap}) coefficients, their wavelength dependence, and the role of the Indo-Gangetic plains (IGP), boundary-layer dynamics (BLD) and long-range transport (LRT) in aerosol evolution via the Atmospheric Radiation Measurement Mobile Facility. The analysis is separated for particles $< 10 \mu\text{m}$ and $< 1 \mu\text{m}$ in diameter in order to examine the influence of particle size on optical properties. The σ_{sp} and σ_{ap} exhibit a pronounced seasonal variation between the monsoon low and post-monsoon (November) high, while the scattering wavelength exponent exhibits higher values during the monsoon, in contrast to the absorption Ångström exponent which maximizes in December–March. The elevated-background measuring site provides the advantage of examining the LRT of natural and anthropogenic aerosols from the IGP and southwest Asia and

the role of BLD in the aerosol lifting processes. The results reveal higher aerosol concentrations at noontime along with an increase in mixing height, suggesting influence from IGP. The locally emitted aerosols present higher wavelength dependence of the absorption in October–March compared to the rather well-mixed and aged transported aerosols. Monsoon rainfall and seasonally changing air masses contribute to the alteration of the extensive and intensive aerosol properties.

1 Introduction

Light scattering and absorption by atmospheric aerosol cause reduction in solar radiation reaching the ground and deterioration of visibility and air quality, modifying the atmosphere's radiative and energy budget (Antón et al., 2012). The backscattering ratio is a crucial variable for quantifying the cooling effect of aerosols on climate. Although it is weakly dependent on aerosol concentration, it provides useful information about the refractive index, angular dependence of scattering, size and shape of aerosols (Gopal et al., 2014). Wide-spread aerosol pollution mostly from anthropogenic sources is a common phenomenon over south Asia with serious effects on atmospheric circulation, climate and human health (Lawrence and Lelieveld, 2010 and references therein). This aerosol-pollution layer, especially over the

Indo-Gangetic plains (IGP), is clearly observed by the satellite imagery as a thick haze layer (atmospheric brown clouds) over the region (Di Girolamo et al., 2004; Ramanathan et al., 2007), spreading also over the Himalayas with significant light absorption due to high black carbon (BC) concentration (Adhikary et al., 2007; Nakajima et al., 2007; Kopacz et al., 2010; Gautam et al., 2011).

During the last decades, the IGP has experienced increasing aerosol and pollutant emissions mainly from anthropogenic sources, fossil-fuel and biofuel combustion and agricultural biomass burning (Lu et al., 2011; Kaskaoutis et al., 2012), which along with the natural dust emissions and long-range transport (LRT) have led to severely turbid atmospheres (Kaskaoutis et al., 2013). As a consequence, aerosols can strongly modify the regional climate via radiative forcing (Ramanathan et al., 2005; Lau et al., 2006; Gautam et al., 2010) and changes in cloud microphysics, monsoon rainfall and dynamics (Randles and Ramaswamy, 2008; Bollasina and Nigam, 2009; Ganguly et al., 2012; Manoj et al., 2011; Dipu et al., 2013). Due to their significant influence on regional weather, climate, monsoon circulation, glaciology and human health, aerosols are systematically examined over the Indian Himalayas, mostly focusing on columnar properties and radiative forcing (Dumka et al., 2006, 2008; Hegde et al., 2007; Guleria et al., 2011 and reference therein), with a few studies on aerosol chemistry (Ram et al., 2008, 2010; Hegde and Kawamura, 2012). In contrast, systematic analysis of near-surface aerosol properties is sparse and mostly performed by an Indian–Finnish research initiative (Hyvärinen et al., 2009, 2011a, 2011b). Furthermore, Raatikainen et al. (2014) examined the influence of boundary-layer dynamics (BLD) and the effect of changes in boundary-layer height (BLH) on aerosol concentrations over the IGP and their transport up to the Himalayan foothills. Panwar et al. (2013) analyzed the evolution of the PM and BC aerosol mass concentrations at Mukteshwar with respect to seasonal variations of BLH, while Komppula et al. (2009) and Neitola et al. (2011) focused on the aerosol size distribution and new particle formation at the same site. These studies corroborate larger aerosol concentrations and new particle formation during the spring period associated with higher BLH and increased influence of transported aerosols.

To improve knowledge of radiative properties of atmospheric aerosols, their origin and spatio-temporal distribution over the Gangetic–Himalayan (GH) region, the Ganges Valley Aerosol Experiment (GVAX) was initiated from June 2011 to March 2012 (Kotamarthi and Satheesh, 2011). The GVAX project was a joint research campaign between the US Department of Energy (DoE) Atmospheric Radiation Measurement (ARM) program and the Indian Institute of Science, Bangalore, conducted at Manora Peak, Nainital, in the central part of the Indian Himalayas (29.21° N, 79.27° E, 1958 m a.s.l.). Based on GVAX measurements, Manoharan et al. (2014) analyzed the aerosol properties, mostly emphasizing the higher absorption of supermicron (1–10 µm) particles

during October–November, which accounts for 44 % of the total aerosol radiative forcing. Dumka and Kaskaoutis (2014) examined the variation of the single-scattering albedo (SSA) during GVAX, its contribution to the aerosol radiative forcing efficiency depending on particle size and some preliminary results of the monthly variation of scattering and absorption coefficients. More recently, Dumka et al. (2015) analyzed the cloud condensation nuclei (CCN) variations and examined the activation of aerosol particles in CCN as a function of season, LRT and BLD.

The present work aims to comprehensively investigate the intensive and extensive aerosol properties (scattering, backscattering and absorption coefficients, their wavelength dependence and the relationships between them) as a function of particle size ($D_{10\mu\text{m}}$ and $D_{1\mu\text{m}}$) over the GH region during the GVAX campaign. The main objective is to shed light on the temporal (diurnal, monthly, seasonal) evolution of the near-surface aerosol properties and the specific role of the BLD, uplift of aerosols, LRT and rainy washout. The nearby background measuring site (Nainital) gives us the possibility of exploring the specific role of aerosol-pollution uplift from the IGP to the Himalayan foothills and the seasonal influence of LRT on aerosol optical properties.

2 Measurements and data analysis

2.1 Observational site

The aerosol measurements were conducted by the DoE/ARM Mobile Facility (AMF) deployed at the (1958 m a.s.l.) Manora peak, Nainital, in the GH region (Dumka and Kaskaoutis, 2014). The observational site is far from any major pollution sources such as industrialized areas and metropolitan cities, with a total population of ~0.5 million and density of ~50 people per km² (census 2011). The site is bounded by high-altitude mountain peaks in the north and east and opens to the IGP region (densely populated, highly polluted and aerosol laden) in the south and west. By considering the elevated nature of the site, the growth of the planetary boundary layer (PBL) in the early afternoon hours (usually up to 3–3.5 km a.s.l.) plays a major role in bringing up aerosols from the IGP, causing significant perturbations in atmospheric physics and chemistry (Dumka et al., 2010; Prabha et al., 2012). The major aerosol sources in Nainital during winter are local/regional biomass burning emissions (domestic use and heating purposes) and transport of pollutants from the IGP (Dumka et al., 2008). During the pre-monsoon period (March–May), the site is influenced by transported dust plumes from the Thar desert and southwest Asia (Hegde et al., 2007; Kumar et al., 2014) with a relative decrease in carbonaceous aerosols (Ram et al., 2008), while in the post-monsoon season, smoke-laden air masses from agricultural crop-residue burning in Punjab affect the

site. The rain-washout process during the monsoon period decreases the aerosol concentration.

2.2 Measurements and techniques

In situ measurements of near-surface aerosol absorption (σ_{ap}) and scattering (σ_{sp}) coefficients were carried out using the aerosol observing system (AOS) (Sheridan et al., 2001; Jefferson, 2011, and references therein). The AOS was housed in an air-conditioned trailer and aerosol samples were obtained from the top of a stainless-steel intake stack (20.3 cm inner diameter), protected with a rain cap. The aerosols were passed from the stack through a manifold and into several sampling lines that deliver the sample air to the various instruments. Each aerosol sample passes through switched impactors that toggle the aerosol size cut between 1.0 μm ($D_{1\mu\text{m}}$) and 10 μm ($D_{10\mu\text{m}}$) aerodynamic particle diameters every 30 min, thus allowing the examination of both fine and coarse particles (Jefferson, 2011). The AOS instrumentation that is used in the current work consists of a nephelometer and a particle soot absorption photometer (PSAP) from which several extensive and intensive aerosol properties have been analyzed (see Table 1).

The σ_{ap} was measured via the three wavelengths (0.47, 0.53 and 0.66 μm) of the PSAP. The PSAP uses a filter-based technique in which aerosols are continuously deposited onto a glass fiber filter and the change in the transmitted light is related to the σ_{ap} of the deposited particles using the Beer–Lambert law (Bond et al., 1999). Absorption data with filter transmissions below 0.7 were rejected in this study, while the data averaging time was 1 min. The response of PSAP depends on aerosol loading on the filter, amount of light scattered by particles, flow rate ($\sim 0.8 \text{ L min}^{-1}$) and spot size (Virkkula et al., 2011). Following the methodology from previous works (Bond et al., 1999; Ogren, 2010), the raw PSAP data were processed to estimate the σ_{ap} by incorporating the sample area, flow rate and spot-size calibrations. Other biases are due to the scattering and multi-sample loading on the filter, instrument noise ($\sim 6\%$ of total absorption; Bond et al., 2001) and uncertainty in the PSAP measurements (1 to 4 Mm^{-1} for the 1 min averaged data samples; Manoharan et al., 2014). The total uncertainty of the PSAP measurements after the transmission and scattering correction is $\sim 20\text{--}30\%$ (Bond et al., 1999).

The total scattering (σ_{sp} ; between 7° and 170°) and hemispheric backscattering (σ_{bsp} ; between 90° and 170°) coefficients at three wavelengths (0.45, 0.55 and 0.70 μm) were measured with an integrating nephelometer (Model 3563, TSI). The nephelometer operated at a relative humidity (RH) below 40% to minimize the effects of changing RH on measurements, while a second nephelometer was also connected to a humidity scanning system to provide measurements of σ_{sp} and σ_{bsp} as a function of RH to study the light scattering enhancement factor (work under preparation). The angular non-idealities (i.e., truncation error) and non-Lambertian

light source were corrected following the methodology described by Anderson and Ogren (1998); details are given in Dumka and Kaskaoutis (2014, and references therein). The averaging time was set to 1 min, and the nephelometer was calibrated using CO_2 as the high span gas and air as the low span gas. On average, the calibration constant is within $\pm 2\%$ and the overall uncertainty in the σ_{sp} is $\sim 7\%$ (Heintzenberg et al., 2006). However, as noticed at the end of the campaign, the CO_2 was too low quality to produce an accurate calibration, thus increasing the uncertainty of the nephelometer measurements to 10–15%.

The aerosol coefficients σ_{sp} , σ_{bsp} and σ_{ap} measured directly by the AOS are referred as “extensive properties” because they mainly pertain to the number of aerosols in the atmosphere. These measurements were used to determine several other aerosol variables (known as “intensive properties”), such as the scattering Ångström exponent (SAE), back-scattering Ångström exponent (BAE), absorption Ångström exponent (AAE), hemispheric backscatter fraction (b), submicron scattering (R_{sp}) and absorption (R_{ap}) fractions, which are involved in the radiative forcing estimations rather than being related directly to the aerosol loading (Table 1). Therefore, the intensive properties relate more to the character of aerosols, such as albedo, particle size and hygroscopic behavior.

3 Results and discussion

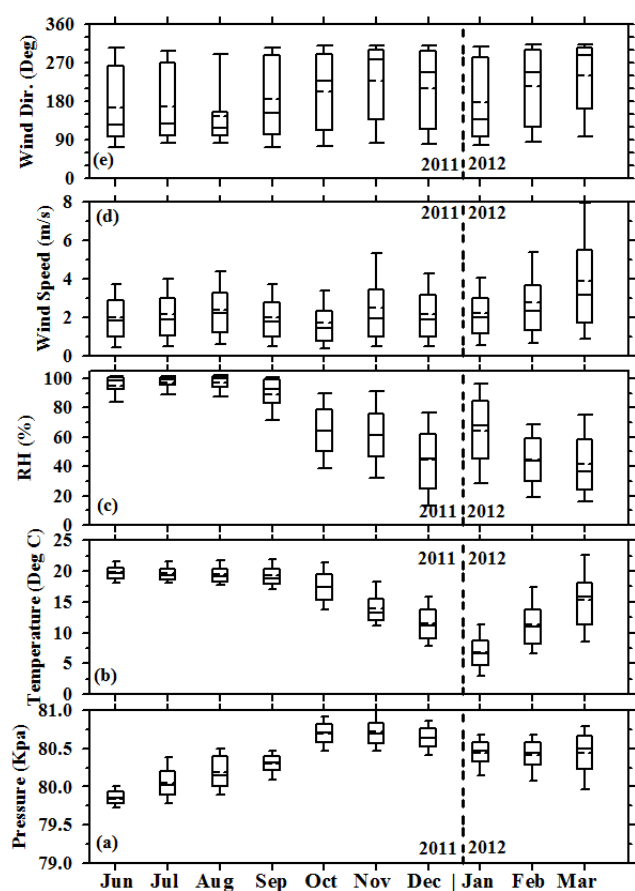
3.1 Variations in meteorological variables

In terms of weather conditions and climatology, the observational site is characterized by four different seasons: winter (December–January–February), spring/pre-monsoon (March–April–May), summer/monsoon (June–July–August–September) and autumn/post-monsoon (October–November). The ambient pressure, temperature, relative humidity, wind speed and wind direction were continuously monitored during the study period (June 2011 to March 2012) using the surface meteorological instrumentation (MET) data from the ARM AMF facility.

The ambient atmospheric pressure varies between 79 and 81 Kpa, gradually increasing from monsoon to winter and then slightly decreasing towards spring (Fig. 1a). The monthly-mean temperature remains nearly steady ($\sim 20^\circ\text{C}$) between June and September, with a gradual decrease thereafter to a minimum value of $\sim 7^\circ\text{C}$ in January (Fig. 1b). The RH is greater than 90% during the summer monsoon and decreases to about 60 to 40% during the rest of the period, also exhibiting a larger fluctuation due to changing weather conditions involving arrival of humid or dry air masses (Fig. 1c). In general, the wind speed (Fig. 1d) varies between 2 and 6 m s^{-1} with an average of $\sim 2 \text{ m s}^{-1}$ most of the time. Westerly to northwesterly winds (Fig. 1e) dominate during the October–March period, carrying aerosols and pol-

Table 1. Details of AOS instruments, variables and equations used for the calculation of aerosol optical properties.

Instruments	Primary measurements	Derived variables	Equation
Three-wavelength nephelometer (TSI Model 3563)	Total scattering and hemispheric backscattering coefficients (σ_{sp} & σ_{bsp}) from D_1 and D_{10} particles at blue (0.45), green (0.55) and red (0.70) μm	Hemispheric backscatter fraction, scattering Ångström exponent, backscattering Ångström exponent and submicron scattering fraction	$b = \sigma_{bsp}/\sigma_{sp}$ $SAE = -\log[\sigma_{sp}(\lambda_1)/\sigma_{sp}(\lambda_2)]/\log[\lambda_1/\lambda_2]$ $BAE = -\log[\sigma_{bsp}(\lambda_1)/\sigma_{bsp}(\lambda_2)]/\log[\lambda_1/\lambda_2]$ $R_{sp} = \sigma_{sp}(D_1)/\sigma_{sp}(D_{10})$
Radiance Research particle soot absorption photometer	Light absorption coefficient (σ_{ap}) from D_1 and D_{10} particles at blue (0.467), green (0.53) and red (0.66) μm	Absorption Ångström exponent and submicron absorption fraction	$AAE = -\log[\sigma_{ap}(\lambda_1)/\sigma_{ap}(\lambda_2)]/\log[\lambda_1/\lambda_2]$ $R_{ap} = \sigma_{ap}(D_1)/\sigma_{ap}(D_{10})$

**Figure 1.** Monthly surface meteorological variables (ambient pressure, air temperature, relative humidity, wind speed and direction) at Nainital during the period June 2011 to March 2012 in box-and-whisker charts. The dashed line represents the mean and the solid line the median. The box contains the range of values from 25 % (bottom) to 75 % (top).

lutants from western IGP and southwest Asia. June is mostly considered a transition month with changing wind from west-

erly to easterly, while the mean wind direction from July to September is easterly to southeasterly, which is associated with increased monsoon rainfall.

3.2 Temporal evolution of near-surface aerosol properties

This section analyzes the temporal evolution of near-surface aerosol properties in Nainital and discusses them as a function of wavelength, particle size and prevailing atmospheric and meteorological conditions.

3.2.1 Extensive properties

The mean values (averaged on a seasonal basis and during the entire study period) of σ_{sp} , σ_{bsp} and σ_{ap} along with their wavelength dependencies are summarized in Table 2 for both $D_{10\mu\text{m}}$ and $D_{1\mu\text{m}}$ particles in order to reveal the influence of particle size on aerosol extensive and intensive properties.

The average σ_{sp} and σ_{ap} during the whole study period were found to be 177.2 Mm^{-1} and 13.5 Mm^{-1} for the $D_{10\mu\text{m}}$ and 104.4 Mm^{-1} and 8.9 Mm^{-1} for the $D_{1\mu\text{m}}$ (Table 2), respectively, with significant seasonal variation (post-monsoon high and monsoon low). The mean value of σ_{sp} is similar to earlier observations over the site (Pant et al., 2006; Beegum et al., 2009). The σ_{sp} values over the central Indian Himalayas (present study and Hyvärinen et al. 2009) are comparable to those found over central India during February 2004 (Jayaraman et al., 2006) but much lower than those ($250\text{--}2000 \text{ Mm}^{-1}$) reported in polluted Indian megacities, like Delhi (Ganguly et al., 2006). The scattering is $\sim 40\%$ larger for the $D_{10\mu\text{m}}$, especially at longer wavelengths, while the σ_{bsp} varies from ~ 5 to 23 Mm^{-1} (~ 3 to 14 Mm^{-1}) for $D_{10\mu\text{m}}$ ($D_{1\mu\text{m}}$) on a monthly basis. The σ_{bsp} follows the seasonal variation of σ_{sp} with larger values in November (~ 0.23 and ~ 0.13 for $D_{10\mu\text{m}}$ and $D_{1\mu\text{m}}$, respectively) and lowest in monsoon season. The monthly variations of the spectral σ_{sp} and σ_{ap} were documented in Dumka and Kaskaoutis (2014). Manoharan et al. (2014) reported a 30 % greater

Table 2. Summary of the extensive and intensive aerosol properties during the GVAX campaign (June 2011–March 2012). The values in parenthesis refer to the $D_{1\mu\text{m}}$ particles.

Parameter	Winter (Dec–Feb)	Pre-monsoon (Mar)	Monsoon (Jun–Sep)	Post-monsoon (Oct–Nov)	Whole period (11 Jun–12 Mar)
σ_{sp} (Mm^{-1}) [0.55 μm]	185.29 \pm 73.46 (122.70 \pm 51.39)	228.95 \pm 65.00 (122.26 \pm 40.01)	113.87 \pm 08.58 (53.97 \pm 5.28)	282.43 \pm 103.25 (158.87 \pm 61.88)	177.2 \pm 157.5 (104.4 \pm 94.2)
σ_{bsp} (Mm^{-1}) [0.55 μm]	13.27 \pm 5.73 (9.58 \pm 3.93)	19.47 \pm 6.18 (11.83 \pm 3.30)	7.46 \pm 5.89 (4.09 \pm 2.65)	19.43 \pm 9.77 (12.10 \pm 5.78)	12.58 \pm 11.46 (8.18 \pm 7.39)
σ_{ap} (Mm^{-1}) [0.53 μm]	11.15 \pm 6.71 (9.20 \pm 5.73)	13.89 \pm 9.37 (10.41 \pm 7.27)	6.21 \pm 1.37 (5.20 \pm 1.30)	16.07 \pm 7.43 (12.17 \pm 5.66)	13.49 \pm 13.02 (8.95 \pm 8.28)
SAE [0.45/0.70 μm]	0.75 \pm 0.05 (1.19 \pm 0.05)	0.44 \pm 0.05 (0.95 \pm 0.05)	0.91 \pm 0.02 (1.42 \pm 0.02)	0.55 \pm 0.04 (1.02 \pm 0.04)	0.72 \pm 0.42 (1.21 \pm 0.35)
BAE [0.45/0.70 μm]	0.31 \pm 0.14 (0.49 \pm 0.13)	0.10 \pm 0.15 (0.34 \pm 0.17)	0.26 \pm 0.26 (0.45 \pm 0.22)	0.13 \pm 0.11 (0.31 \pm 0.09)	0.24 \pm 0.21 (0.42 \pm 0.18)
AAE [0.47/0.66 μm]	1.25 \pm 0.07 (1.29 \pm 0.04)	1.27 \pm 0.09 (1.34 \pm 0.08)	0.93 \pm 0.05 (0.96 \pm 0.04)	1.11 \pm 0.08 (1.22 \pm 0.04)	1.07 \pm 0.20 (1.14 \pm 0.18)
b [0.55 μm]	0.072 \pm 0.012 (0.083 \pm 0.014)	0.084 \pm 0.001 (0.096 \pm 0.011)	0.057 \pm 0.012 (0.063 \pm 0.012)	0.069 \pm 0.013 (0.077 \pm 0.001)	0.067 \pm 0.009 (0.073 \pm 0.012)
R _{sp} [0.55 μm]	0.67 \pm 0.08	0.54 \pm 0.08	0.60 \pm 0.18	0.58 \pm 0.09	0.61 \pm 0.13
R _{ap} [0.53 μm]	0.83 \pm 0.07	0.75 \pm 0.07	0.88 \pm 0.11	0.77 \pm 0.09	0.83 \pm 0.11

absorption for $D_{10\mu\text{m}}$ compared to $D_{1\mu\text{m}}$ during October–November 2011, in contrast to the similar values (7.63 ± 5.32 and 6.38 ± 3.91 for $D_{10\mu\text{m}}$ and $D_{1\mu\text{m}}$, respectively) found during the monsoon. The post-monsoon season coincides with the post-harvest agricultural biomass burning period in Punjab, northwestern India (Kaskaoutis et al., 2014), implying that the absorbing aerosols can also be of larger size due to atmospheric mixing and ageing processes (gas-to-particle conversion, coagulation, condensation) during their transportation up to Nainital. These aerosols are mostly emitted over IGP, whereas the local freshly emitted aerosols in Nainital (mostly in the $D_{1\mu\text{m}}$ size) seem not to affect the light absorption as much due to their significantly lower abundance (Hyvärinen et al., 2009; Ram et al., 2010). It should be noted that the difference in absorption coefficient between $D_{10\mu\text{m}}$ and $D_{1\mu\text{m}}$ is larger for higher aerosol loading post-monsoon and in March.

Higher values of σ_{bsp} ($14 \pm 1 \text{ Mm}^{-1}$) and b (~ 0.13) at 550 nm compared to Nainital were found in Anantapur, south India, during January–December 2011 (Gopal et al., 2014), suggesting dominance of different aerosol types associated with lower aerosol loading (mean σ_{sp} of $97 \pm 9 \text{ Mm}^{-1}$). σ_{sp} value of $75 \pm 42 \text{ Mm}^{-1}$ at 550 nm was reported by Andreae et al. (2002) in Sde Boker, Israel, which was typical of moderately polluted continental air masses, while values of 26 Mm^{-1} and 410 Mm^{-1} were found for clean and heavy-

smog days, respectively, in Los Angeles (Seinfeld and Pandis, 1998). Table 3 summarizes the extensive and intensive aerosol properties over Nainital during the GVAX campaign along with those measured over mountainous and remote sites over the globe. The comparison shows that Nainital, despite its elevated terrain and remoteness from urban and industrialized regions, usually receives substantial amounts of anthropogenic aerosols in addition to mineral dust and biomass burning, rendering the site moderately polluted.

3.2.2 Intensive properties

The monthly values of SAE determined at three spectral bands are shown in Fig. 2, exhibiting a similar temporal variation for both $D_{1\mu\text{m}}$ and $D_{10\mu\text{m}}$ size groups but with much larger values for the $D_{1\mu\text{m}}$ (mean of 1.21 ± 0.35 at 0.45–0.70 μm) compared to $D_{10\mu\text{m}}$ (mean of 0.72 ± 0.42 at 0.45–0.70 μm) (Table 2). The wide range (~ 0.1 to 2.4) of SAE values for both particle groups suggests large variability in sources, seasonality and mixing processes at the measuring site. The average value of SAE at 0.45–0.70 μm was found to be 1.02 ± 0.30 at Anantapur (Gopal et al., 2014), which is well within the average values of $D_{1\mu\text{m}}$ and $D_{10\mu\text{m}}$ in Nainital. Furthermore, the SAE values are higher at the shorter wavelength bands, suggesting a higher decreasing rate of the scattering process at shorter wavelengths, as expected from the Mie theory. Previous work (Dumka and Kaskaoutis 2014)

Table 3. Comparison of extensive and intensive aerosol properties over Nainital during the GVAX campaign along with those measured over mountainous or remote areas over the globe.

Sampling Site	Elevation (m)	Sampling Period	σ_{sp} (Mm^{-1})	σ_{ap} (Mm^{-1})	SAE	AAE	Reference
Nainital, India	1958	11 June–12 March	177.20 (104.40)*	13.49 (8.95)*	0.72 (1.21)*	1.07 (1.14)*	Present study
Nainital, India	1958	5 Feb–8 Jul	–	13.9	–	–	Ram et al. (2010)
Nainital, India	1958	Dec 2004	–	12.9	–	–	Ram and Sarin (2009)
Nainital, India	1958	5 Feb–7 Jun	–	12.2	–	–	Ram and Sarin (2009)
Mukteshwar, India	2180	5–7 Sep	53.00	11.00	–	1.0–1.6	Hyvärinen et al. (2009)
Mukteshwar, India	2180	2006 to 2009	34.30–133.80	6.90–25.8	–	–	Hyvärinen et al. (2011b)
NCO-P	5079	May–Sep 2006	–	1.1	–	–	Marcq et al. (2010)
Mt. Abu, India	1700	5 Dec–6 Feb	–	8.0	–	–	Ram and Sarin (2009)
Mt. Abu, India	1700	5 May–6 Feb	–	5.8	–	–	Ram and Sarin (2009)
Jungfrauoch, Swiss Alps	3580	5–11 May 2001	~2–11	~0.2–8	~0.5–2.2	~0.9–2.1	Collaud Coen et al. (2004)
Jungfrauoch, Swiss Alps	3580	May 2008***	11.9	–	1.79	–	Fierz-Schmidhauser et al. (2010)
		May 2008**	20.5	–	1.67	–	Fierz-Schmidhauser et al. (2010)
Mauna Loa, USA	3400	^a 2000–2009	1.92(1.24)	0.07(0.07)	1.53(1.35)	–	Andrews et al. (2011)
Whistler, Canada	2200	^b 2008–2009	3.98(3.95)	0.54(0.53)	2.01(2.01)	–	Andrews et al. (2011)
Mount Bachelor, USA	2800	^c April–May 2008–2009	5.32(3.50)	1.00(0.77)	2.54(2.50)	–	Andrews et al. (2011)
Southern Great Plains of Oklahoma		^d 2000–2007	13.00(5.73)	0.77(0.49)	2.09(1.89)	–	Andrews et al. (2011)
Bondville, Illinois		^d 2006–2009	15.30(4.89)	1.00(0.31)	1.91(1.38)	–	Andrews et al. (2011)
Izana, Spain	2400	^a 2008–2009	9.32(6.57)	0.71(0.43)	0.73(0.63)	–	Andrews et al. (2011)
Jungfrauoch, Switzerland	3600	^e 1995–2007	3.50(5.87)	0.50(0.42)	1.85(1.75)	–	Andrews et al. (2011)
Monte Cimone, Italy	2200	^e 2007–2009	17.20(14.30)	2.45(2.00)	–	–	Andrews et al. (2011)
Moussala Peak, Bulgaria	2400	^e 2007–2009	16.00(12.20)	–	2.20(2.12)	–	Andrews et al. (2011)
NCO-P	5079	^f 2006–2008	17.40(10.70)	1.63(0.97)	1.59(1.22)	–	Andrews et al. (2011)
Mount Waliguan, China	3800	^a 2005–2008	42.50(39.70)	2.31(1.94)	0.89(0.85)	–	Andrews et al. (2011)
Mt. Lulin, Taiwan	2900	^a 2008–2009	25.80(10.80)	2.83(0.97)	1.57(1.51)	–	Andrews et al. (2011)
Montsec Western Mediterranean Basin	1570	11 Jun–13 Jun	25.4 ± 27.5	1.5 ± 1.4	1.56 ± 0.88	–	Pandolfi et al. (2014)
Cape Cod, USA	20	12 Jul–13 Jul	22 ± 15	1.1 ± 0.9	1.8 ± 0.6	–	Titos et al. (2014a)
Granada, Spain	680	Winter 2013	41 ± 34	17 ± 17	1.8 ± 0.4	–	Titos et al. (2014b)
Granada, Spain		Spring 2013	38 ± 26	11 ± 11	1.8 ± 0.3	–	Titos et al. (2014b)

* Value inside parenthesis represents for $D_{1\mu m}$ size aerosols. **Value excluding Saharan dust event. ***Value exclusively for Saharan dust event. ^a Size cut (10 μm); ^b size cut (2.5 μm); ^c size cut (1.0 μm); ^d size cut (7.0 μm); ^e whole air; ^f size cut (2.5 μm for scattering) and size cut (10.0 μm for absorption). Values taken from Andrews et al. (2011) are in STP and values inside the parentheses represent free troposphere.

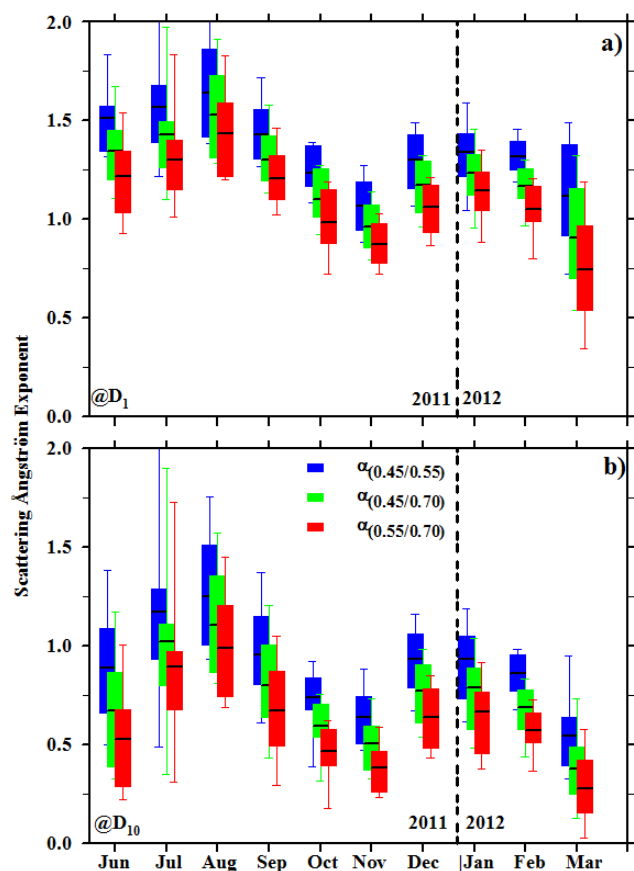


Figure 2. Monthly-mean variation of scattering Ångström exponent for $D_{1\mu\text{m}}$ (a) and $D_{10\mu\text{m}}$ (b) during June 2011 to March 2012. The box-and-whisker plots denote the 95th and 5th percentiles, respectively. The box's upper and lower limits are the 75th and 25th percentiles; the straight black line shows the mean value and the vertical dotted line separates the years 2011 and 2012.

showed a similar annual pattern of σ_{sp} and σ_{ap} for both $D_{1\mu\text{m}}$ and $D_{10\mu\text{m}}$ particles. The present analysis revealed different values and wavelength dependence, indicating that the particle size plays a prominent role in altering the aerosol optical properties.

The monthly variability depends on the dominant aerosol type, the contribution of local and transported aerosols, the prevailing meteorological conditions and the mixing processes in the atmosphere. The maximum monthly-mean SAE is observed in August (1.11 ± 0.31 and 1.53 ± 0.26 for $D_{10\mu\text{m}}$ and $D_{1\mu\text{m}}$, respectively) and, in general, the wavelength dependence of scattering seems to be higher during the monsoon (Table 2). The minimum values are shown in October and November, when the site is under significant influence of the smoke-laden air masses from northwestern India, and both scattering and absorption are at their highest levels (Manoharan et al., 2014; Dumka and Kaskaoutis, 2014). Hyvärinen et al. (2009) found the lowest values of the Aitken-to-accumulation mode ratio during the pre- and

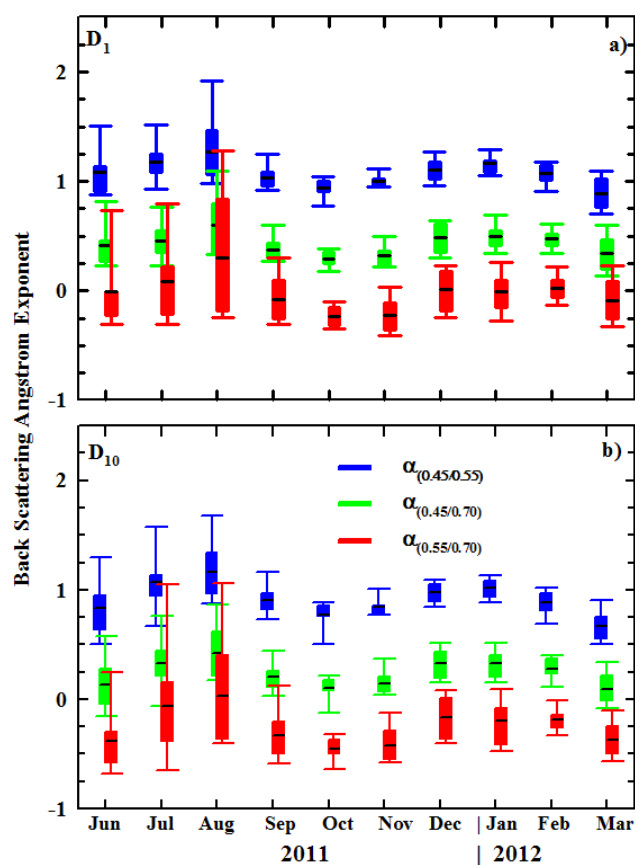


Figure 3. Same as in Fig. 2 but for the back-scattering Ångström exponent.

post-monsoon seasons over the central Indian Himalayas, indicating the largest influence of LRT, which was also justified by the highest particle number concentrations (Dumka et al., 2015). In contrast, during the monsoon season the Aitken-to-accumulation mode ratio was higher due to more efficient removal of accumulation mode by the rain-washout process, implying that the aerosols are of smaller size, less aged and mostly freshly emitted, thus explaining the highest SAE values during July–September. The lowest SAE in November is an indicator of the abundance of aged coarse aerosols, whereas the local primary emissions are mostly at the Aitken size, thus contributing to the much larger SAE for the $D_{1\mu\text{m}}$ particles and to the general increase in SAE during winter due to the influence of biofuel burning. Similar values of SAE, but with a different annual pattern (maximum of 1.5 ± 0.1 in January and minimum of 0.7 ± 0.1 in September), were found in Anantapur (Gopal et al., 2014) indicating significant difference in source apportionment, influence of local emissions and seasonal meteorological conditions between the GH region and the southern Indian peninsula.

The monthly variation of BAE is shown in Fig. 3, revealing a general agreement with SAE (Fig. 2) due to the reasons mentioned above. BAE exhibits significant spectral de-

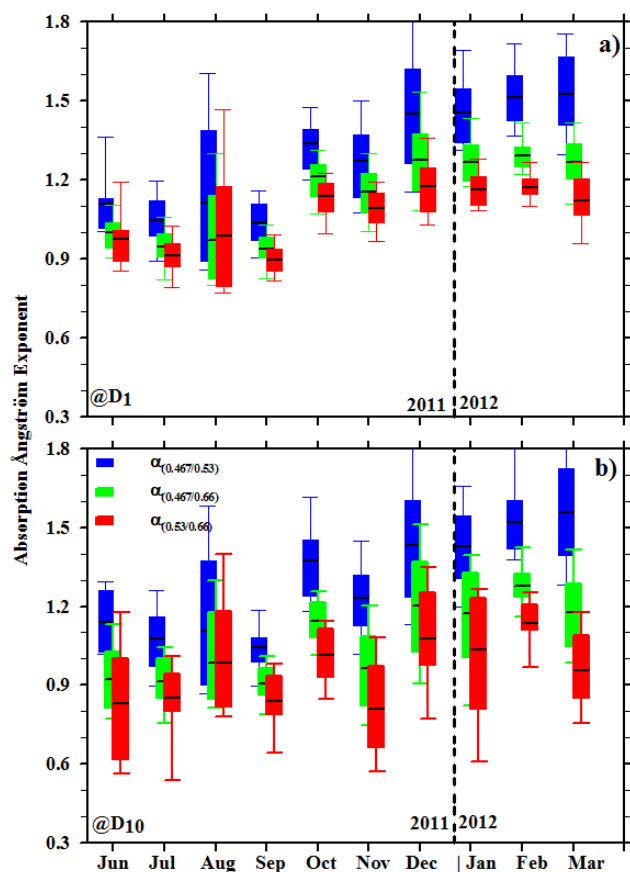


Figure 4. Same as in Fig. 2 but for the absorption Ångström exponent.

pendence with larger values at shorter wavelengths (0.45–0.55 μm) and near zero to even negative values at 0.55–0.7 μm due to larger backscatter coefficient values at 0.7 μm in some months. Note also that the negative $\text{BAE}_{0.55/0.7}$ values are more prominent for $D_{10\mu\text{m}}$ particles, indicating the influence of the particle size in the spectral backscatter coefficient. In contrast, for $D_{1\mu\text{m}}$ particles negative monthly-mean $\text{BAE}_{0.55/0.7}$ values are shown only in October–November and March, i.e., the months with the lowest SAE values (Fig. 2). $\text{BAE}_{0.45/0.7}$ is almost double for the $D_{1\mu\text{m}}$ particles (Table 2) and, especially in seasons with dominance of coarse aged aerosols (pre-monsoon and post-monsoon), the difference between $D_{1\mu\text{m}}$ and $D_{10\mu\text{m}}$ BAE values is even larger. This suggests that BAE is more sensitive to particle size than SAE and can be used as an additional tool for aerosol type discrimination. It was found (not presented) that BAE and SAE are highly linearly correlated to each other with R^2 of 0.8 (0.6) for $D_{10\mu\text{m}}$ ($D_{1\mu\text{m}}$) at 0.45–0.7 μm band, implying covariance in the wavelength dependence of scattering and backscattering.

The monthly variation of the spectral AAE exhibits similar pattern for both size groups with larger values at shorter wavelengths (Fig. 4). However, the wavelength dependence

of the AAE strongly differentiates as a function of season and particle size. It is higher for $D_{10\mu\text{m}}$ particles and increases from monsoon to winter and pre-monsoon (for both particle groups), suggesting differences in the source regions and dominant aerosol type. The larger values and wavelength dependence of AAE correspond to enhanced contribution of dust and carbonaceous aerosols from biofuel burning, while values of AAE around 1 are characteristic of a dominance of fossil-fuel combustion (Kirchstetter et al., 2004). The highest wavelength dependence of AAE in March is a fingerprint of the larger dust contribution either emitted locally or transported long range. The AAE for the $D_{1\mu\text{m}}$ is found to be slightly larger (mean of 1.14 ± 0.18 at 0.47–0.60 μm) than that of $D_{10\mu\text{m}}$ (mean of 1.07 ± 0.20 at 0.47–0.60 μm), with a maximum during December–March (~ 1.3) and minimum during the monsoon (~ 1.0). Monthly-mean AAE values in the range of 1.0 to 1.6 are reported at Mukteshwar, close to Nainital (Hyvärinen et al. 2009), that are larger during winter, similar to our results (Fig. 4). A wide range (from 0.16 to 2.16, mean of 1.43 ± 0.41) in AAE values was also found by Andreae et al. (2002), indicative of very contrasting air masses and aerosol absorption efficiencies in arid Israel. The AAEs for $D_{1\mu\text{m}}$ and $D_{10\mu\text{m}}$ have shown a correlation coefficient of ~ 0.9 and most of the data points lie close to the 1–1 line (Manoharan et al., 2014), suggesting consistency in the aerosol source regions and negligible effect of the particle size. To summarize, the increase in both absorption and scattering coefficients during the last weeks of October and November due to enhanced biomass burning activity over northwestern India is generally associated with a weaker wavelength dependence of both scattering (Fig. 3) and absorption (Fig. 4), suggesting an abundance of supermicron aerosols that absorb in the whole spectrum (Manoharan et al., 2014).

The monthly evolution of the spectral backscatter fraction (b) is shown in Fig. 5 for both particle sizes. The results show that the b is strongly wavelength dependent, with larger values at longer wavelengths (opposite to the results for σ_{sp} and σ_{ap} , SAE and AAE). The larger SAE found during the monsoon (Fig. 2) indicates particles of smaller size, which are associated with more isotropic scattering and usually higher b values, while forward scattering and smaller b values are indicative of larger particles (Mie theory). However, the results exhibit smaller b during the monsoon (Table 2), while the b slightly increases post-monsoon until March (except for small decreases in November and January). The highest b values are observed in March, suggesting a more irregular type of scattering and favoring of backscatter which is characteristic of the dust particles (Liu et al., 2008). Lack of covariance between SAE and b is indicative of a bimodal size distribution, which seems to be the usual scenario in our case. The b is larger at longer wavelengths, especially for the $D_{1\mu\text{m}}$ particles, since the backscatter wavelength dependence is lower than that of total scattering and, therefore, the backscatter-to-total-scattering ratio (b) is more enhanced at

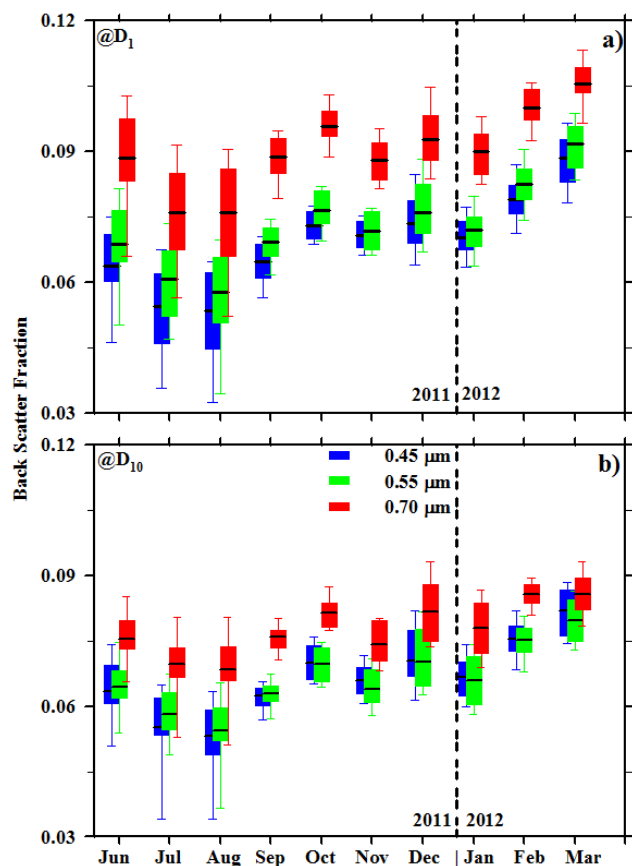


Figure 5. Same as in Fig. 2 but for the back-scatter fraction.

longer wavelengths. Slightly higher b values are found for the submicron particles over Nainital at 0.45 and 0.55 μm (Table 2), which become significantly higher at 0.7 μm compared to those of $D_{10\mu\text{m}}$ (Fig. 5). This is because the coarse particles favor the forward scattering (i.e., larger asymmetry factor and smaller b) than the smaller particles. The b at 0.55 μm lies in the range of 0.034–0.089 (0.027–0.100) with higher values in March 0.080 ± 0.005 (0.092 ± 0.006) and lower in August 0.054 ± 0.010 (0.058 ± 0.012) for $D_{10\mu\text{m}}$ ($D_{1\mu\text{m}}$). On average, the b values at 0.55 μm were found to be 0.067 ± 0.009 for $D_{10\mu\text{m}}$ and 0.073 ± 0.012 for $D_{1\mu\text{m}}$, which are much lower than those (0.13 ± 0.09) reported at Anantapur (Gopal et al., 2014), suggesting the presence of more aged aerosols and a larger size over Nainital. A backscatter ratio value of 0.13 was reported in the Negev desert, Israel, under continental pollution conditions (Formenti et al., 2001; Andreae et al., 2002), while similar values (0.14 ± 0.02) were found for polluted air masses in the northwestern and eastern United States (Anderson et al., 1999; Sheridan and Ogren, 1999). Previous studies (Carrico et al., 2003; Doherty et al., 2005) have shown that the b values are higher for dust and biomass burning aerosols, while they may be also sensitive to composition (organic content and particle size distribution) of aerosols (Twardowski et al., 2001; Boss et al., 2004).

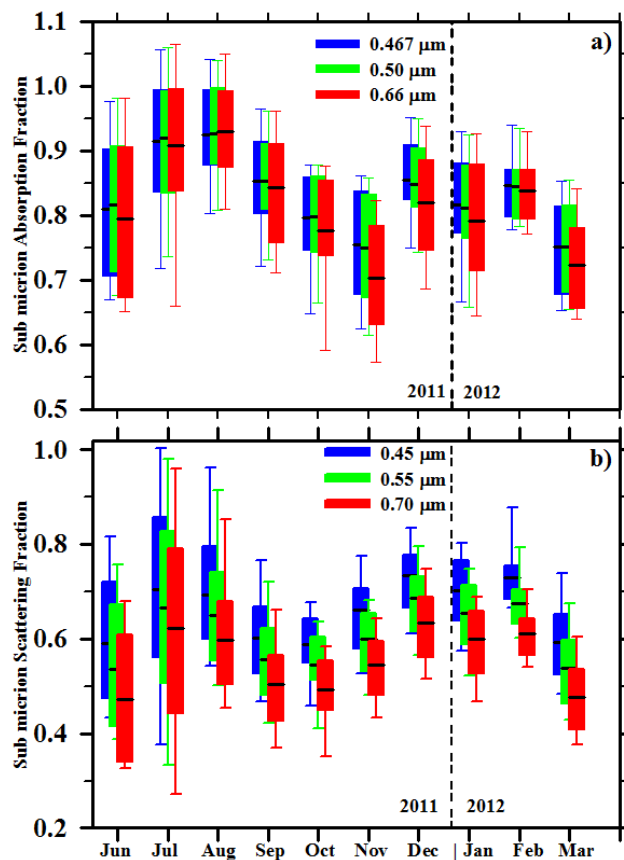


Figure 6. Same as in Fig. 2 but for the submicron absorption (a) and scattering (b) fraction.

Figure 6 shows the temporal evolution of the σ_{sp} and σ_{ap} for the submicron ($D_{1\mu\text{m}}$) particles as a fraction of the respective efficiencies of $D_{10\mu\text{m}}$ (i.e., $D_{1\mu\text{m}}/D_{10\mu\text{m}}$). The decreasing trend with the wavelength for the submicron scattering fraction implies more wavelength sensitivity compared to $D_{10\mu\text{m}}$, whereas it becomes rather neutral for the absorption, suggesting that the spectral absorption is similar for both $D_{1\mu\text{m}}$ and $D_{10\mu\text{m}}$. The submicron absorption fraction is higher than that of scattering, suggesting that the SSA would be lower for $D_{1\mu\text{m}}$ as justified (SSA for $D_{1\mu\text{m}} = 0.91$, SSA for $D_{10\mu\text{m}} = 0.93$) in a previous study (Dumka and Kaskaoutis, 2014).

Both absorption and scattering submicron fractions exhibit a similar pattern with higher values during July–August, a decrease post-monsoon, an increase again in December–January and a decrease in March. The larger SAE during the monsoon (Fig. 2) implies an abundance of fine aerosols (large Aitken-to-accumulation ratio; Hyvärinen et al., 2009), leading to enhanced submicron scattering. The concurrent high values of submicron absorption fraction in July–August suggest that either $D_{1\mu\text{m}}$ particles are more absorbing than during the rest of the year or $D_{10\mu\text{m}}$ would be less absorbing during the monsoon. Submicron scattering and absorp-

tion are sensitive to the local anthropogenic emissions (at the Aitken size) during the monsoon and winter months, thus exhibiting higher fractions compared to the rest of the period. Except for the particle size and shape that mostly define the scattering processes, the aerosol chemical composition plays a vital role in the absorption efficiency. The carbonaceous aerosols were found to contribute about 25 % of the total aerosol mass in Nainital (Ram et al., 2010), while the water-soluble organic carbon/organic carbon ratio (0.55 ± 0.15) was found to be larger than that over the IGP locations, suggesting enhanced contribution from secondary organic aerosols (mostly in the Aitken size). Concerning the coarse-mode particles, except for the LRT dust from the arid and semi-arid regions in southwestern Asia (see Fig. 9), dust particles may originate from local wind-blown dust, dust re-suspension due to road traffic or dust due to farming activities over the GH region (Raatikainen et al., 2014).

3.3 Diurnal cycle of aerosol properties

The monthly-mean diurnal evolutions of σ_{sp} , σ_{ap} , SAE and AAE are shown in Fig. 7 for both $D_{1\mu\text{m}}$ and $D_{10\mu\text{m}}$. The σ_{sp} and σ_{ap} exhibit similar diurnal and seasonal patterns, with highs post-monsoon until winter (and March) and lows during the monsoon. Both maxima are observed in November, caused by significant influence of transported smoke from agricultural burning (Dumka and Kaskaoutis, 2014), while a slight decrease is observed in January. Similar annual variation of both σ_{sp} and σ_{ap} was reported in Mukteshwar (Hyvärinen et al. 2009). The slightly lower December–January values were attributed to the confinement of the IGP polluted boundary layer below the site's altitude. Furthermore, synoptic-scale transport and changing air-mass origin affect the aerosol loading over the Himalayan sites (Xu et al., 2014; Bucci et al., 2014). The annual variation of the σ_{ap} seems to follow that of the BC mass fraction, which was found to be $\sim 1\%$ during the monsoon and 7.6% during winter (Ram et al., 2010) associated with variation in σ_{ap} (at $0.678\mu\text{m}$) from 0.9 to 33.9Mm^{-1} . However, no significant difference in σ_{ap} and σ_{sp} was found between weekdays and weekends, in contrast to Anantapur, where a 7.8% reduction in σ_{sp} was reported on weekends (Gopal et al., 2014). The factor that seems to contribute to the increase in σ_{sp} and σ_{ap} from noontime to afternoon hours it is the upstream slope of the polluted air masses coming from the IGP after a deepening ($>2.5\text{--}3\text{ km}$) of the PBL over the Ganges valley. Local-scale daily wind patterns, like valley wind cells, may also influence the diurnal patterns of spectral σ_{sp} and σ_{ap} ; upslope winds are expected to increase the aerosol loading over the site, while downslope winds result in atmospheric cleansing. Afternoon-to-evening peaks in σ_{sp} and σ_{ap} , which vanished during monsoon, were also reported at Mukteshwar during the post-monsoon and winter seasons (Hyvärinen et al. 2009).

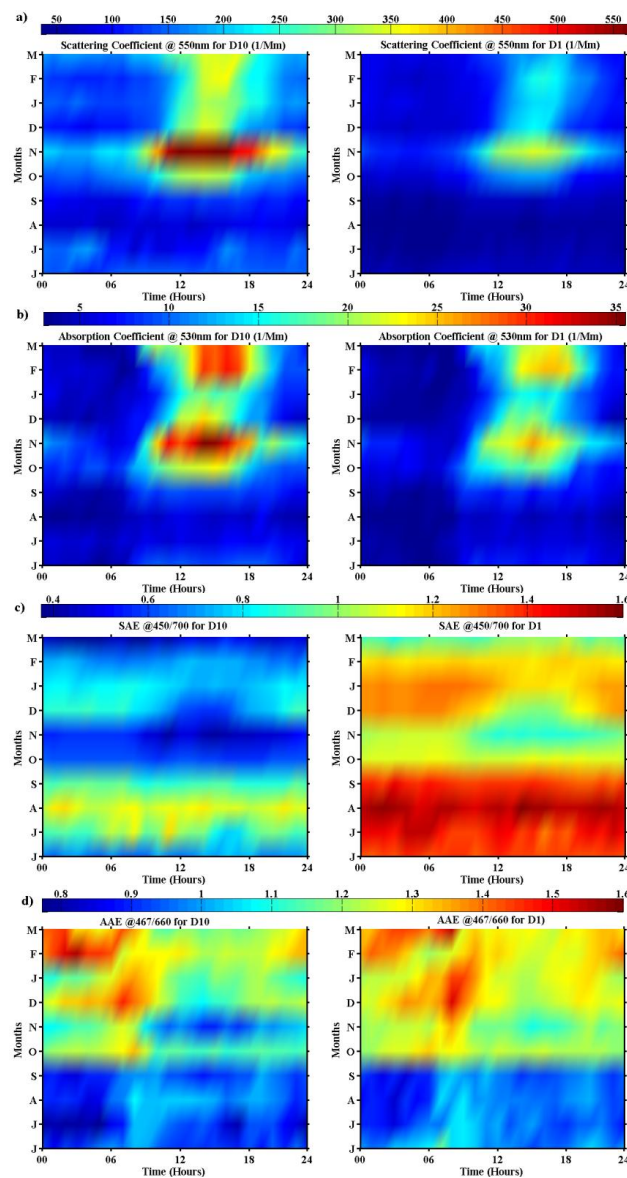


Figure 7. Monthly-mean diurnal variation of (a) scattering coefficient, (b) absorption coefficient, (c) scattering Ångström Exponent (SAE) and (d) absorption Ångström Exponent (AAE) for $D_{10\mu\text{m}}$ and $D_{1\mu\text{m}}$ size particles.

The seasonal pattern of SAE reveals larger values during the monsoon, which can be explained by the rain washout of the coarser aerosols and a secondary increase during December–January mostly associated with local emissions from biofuel combustion (morning and evening maxima). The diurnal variation observed in December–January is smoothed during the rest of the year for both particle sizes. In contrast to SAE, the diurnal pattern of AAE exhibits significant variability during October–March, indicating dominance of different aerosol types and mixing processes. Higher AAE values ($>1.3\text{--}1.4$) are observed during

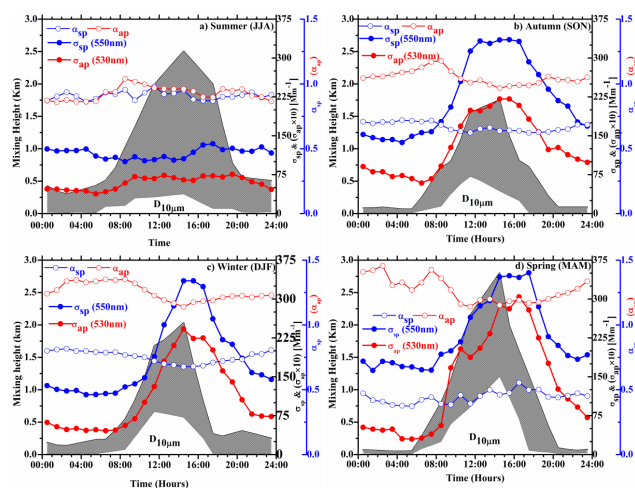


Figure 8. Diurnal variation of the seasonal mean scattering, absorption coefficients, SAE and AAE for $D_{10\mu\text{m}}$ particles along with respective variations in the maximum and minimum mixing-layer height over Nainital. The absorption coefficient was multiplied by 10.

night-to-early-morning hours in the winter season, while the AAE goes down to 1–1.2 at noontime. Peaks in AAE during the morning and evening hours were also found over Mukteshwar (Hyvärinen et al. 2009) suggesting influence of local biomass burning, i.e., burning of leaves and wood for heating, which did not contribute to the diurnal patterns of σ_{sp} and σ_{ap} (Fig. 7a, b), as they are mostly affected by the LRT from IGP. The diurnal pattern of AAE reveals the dominance of different aerosol sources and combustion processes, i.e., local emissions from biofuel burning in the early morning and evening hours (high values of AAE) and transport of mostly aged aerosols from fossil-fuel combustion in IGP from noontime to early afternoon (low values of AAE) (Bergstrom et al., 2007). In contrast, any diurnal pattern flattens out during a monsoon, when the low AAE values (below 1) are associated with lowest σ_{ap} .

Raatikainen et al. (2014) noted that during winter the air masses up to Himalayan sites travel at higher altitudes than the maximum BLH ($\sim 1\text{--}1.5\text{ km}$) over the IGP, thus not being able to carry a significant amount of aerosol and pollutants. Such pollution transportation is very much favored pre-monsoon when the BLH is at its maximum ($> 3\text{--}3.5\text{ km}$) and the dilution of aerosols in the vertical favors their uplift to Himalayan foothills. Therefore, the role of the IGP in the aerosol concentrations over the Himalayas is strongly related to BLH and dynamics. Figure 8 summarizes the seasonal-mean diurnal variations of σ_{sp} , σ_{ap} , SAE and AAE for $D_{10\mu\text{m}}$ along with that of BLH. The latter was obtained from the HYSPLIT model on an hourly basis using the turbulent kinetic energy (TKE) profile method (Draxler et al., 2012), supposing that the BLH is assigned to the height at which TKE either decreases by a factor of 2 or to a value less than

$0.21\text{ (m}^2\text{ s}^{-2}\text{)}$. The BLH exhibits a pronounced diurnal variation in all seasons, especially pre-monsoon (March) when it can reach up to 2.7 km in early afternoon hours. During nighttime and early morning the BLH is only a few meters, thus trapping aerosols and pollutants near the ground.

The diurnal variation of the σ_{sp} and σ_{ap} exhibits a systematic increase during noon-to-early-afternoon hours, coinciding well with the maximum BLH. In contrast, numerous papers (Ganguly et al., 2006; Beegum et al., 2009; Srivastava et al., 2012; Dumka et al., 2013; Pathak et al., 2013; Gopal et al., 2014, and many references therein) have shown increased pollutant (mostly emphasizing BC) concentrations over Indian cities during early morning and evening hours due to lower BLH and trapping of pollutants near the ground and lower concentrations at noontime (maximum BLH) due to enhanced convection and dilution of pollutants. These diurnal patterns correspond mostly to urban environments and enhanced local emissions. The contrasting diurnal variation of σ_{sp} and σ_{ap} in Nainital suggests dominance of long-range transported aerosols from the Ganges basin and west Asia, since the uplift is favored by the deeper mixing layer at noontime. Note also a small time lag between maximum in BLH and aerosol scattering/absorption that exists 1–2 h later. In contrast, the diurnal variation is nearly vanished during the monsoon due to rainy washout, which seems to smooth the effect of the LRT and constitutes the most effective scavenging factor that controls the aerosol loading and evolution. Prabha et al. (2012) revealed the removal of pollution from the IGP to higher atmospheric levels in association with dynamically forced updrafts. Their results showed that the valley pollution could be uplifted to heights above the haze layer, favored by the buoyancy generated due to thermal heating of the surface during noon-to-early-afternoon hours. Similar diurnal patterns of BC and aerosol concentrations were found over other Himalayan sites, like the Nepal Climate Observatory – Pyramid (NCO-P), Nepal, and Darjeeling, in the eastern Indian Himalayas (Marinori et al., 2010; Sarkar et al., 2014). In contrast, the diurnal patterns of SAE and AAE do not exhibit significant variations in all seasons, although the slightly higher values observed during early morning suggest local influence of fine, freshly emitted aerosols.

3.4 The role of wind and LRT in aerosol properties

The diurnal and seasonal evolution of the aerosol properties over Nainital is a function of the emission sources, meteorological conditions (rainfall, wind pattern), BLD and LRT. In this respect, the variation in σ_{sp} , σ_{ap} , SAE and AAE is examined against the wind speed and direction (Fig. 9). In general, the results show that the west/southwest flow enhances the scattering and absorption coefficients, while the north air masses are mostly clean. The air flow from the southeast is mostly associated with the monsoon circulation, higher rainfall and lower aerosol concentrations; however, it was found that the concentrations from this sector are similar to those

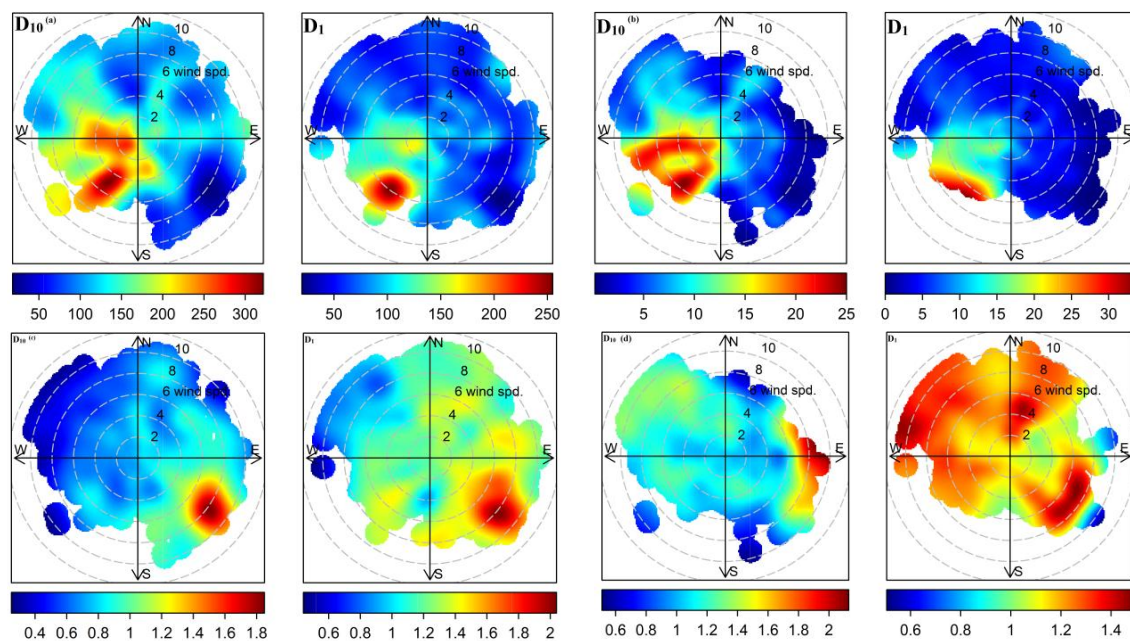


Figure 9. Bivariate plots of the scattering coefficient (a), absorption coefficient (b), scattering Ångström exponent (c) and absorption Ångström exponent (d) for $D_{10\mu\text{m}}$ and $D_{1\mu\text{m}}$ size groups.

from the southwest during the other seasons. Similar findings (lower values for both scattering and absorption associated with east/southeast directions) were found in Mukteshwar (Hyvarinen et al., 2009), while the highest values were found for western and southwestern sectors. The maximum σ_{sp} and σ_{ap} values are mostly associated with moderate winds ($4\text{--}6\text{ ms}^{-1}$), supporting the higher contribution of the transported aerosols at the observational site. In contrast, the accumulation of pollutants over the urban areas is favored by calm winds resulting in larger values of σ_{sp} (almost double for wind speed $<0.5\text{ m s}^{-1}$ compared to wind speed $>3\text{ m s}^{-1}$) at Anantapur (Gopal et al., 2014). The east flow carries smaller particles with SAE greater than 1.2, which can be up to 1.6–1.8 for certain air masses from the southeast; in contrast, the northwest sector is associated with larger particles (much lower values of SAE). However, the AAE is not so much dependent on the wind direction, revealing larger influence by the local emissions as discussed in Fig. 7. The valley-breeze circulation was found to have a strong impact on the aerosol composition even at the high-altitude (5079 m) NCO-P site in the Everest area (Decesari et al., 2010) and, therefore, is considered the major mechanism for the aerosol transport from the polluted IGP up to Himalayas. This was further supported by chemical analysis of the water-insoluble organic carbon/elemental carbon ratios between Nainital and IGP (Ram and Sarin, 2010), which revealed aerosol of similar sources. To summarize, seasonal changes in meteorology conditions, air-mass origin and transport pathways as well as variations in BLH influence the scattering, absorbing coefficients and their wavelength dependence in Nainital. Various

synoptic weather conditions and changes in BLH were also found to play an emerging role in aerosol properties at the high-altitude Jungfrauoch site in the Swiss Alps (Collaud Coen et al., 2011).

The whole analysis revealed that the BLD and LRT play the major role in the aerosol field and temporal evolution over Nainital in all seasons except monsoon, when the rain washout is the main process. The potential aerosol source regions are difficult to define by simple air-mass back trajectories or even trajectory clusters. Therefore, an advanced technique (concentrated weighted trajectory, CWT), which is able to quantify the regional contribution of each of advection pathway to the measured aerosol variable (Seibert et al., 1994; Dumka et al., 2013), was performed by combining statistical analysis of back trajectories with the aerosol properties (σ_{sp} , σ_{ap} , SAE and AAE). The trajectories ending at 500 m over Nainital were weighted on the basis of the measured aerosol properties during their arrival and each grid cell is assigned a concentration obtained by averaging trajectory-associated concentrations that had crossed the grid cell (Fig. 10a–d):

$$C_{ij} = \frac{1}{\sum_{l=1}^M \tau_{ijl}} \sum_{l=1}^M C_l \tau_{ijl}, \quad (1)$$

where C_{ij} is the average weighted concentration in a grid cell (i, j), C_l is the measured variable, τ_{ijk} is the number of k^{th} trajectory endpoints in the (i, j) grid cell and M is the total number of trajectory endpoints in the (i, j) grid cell

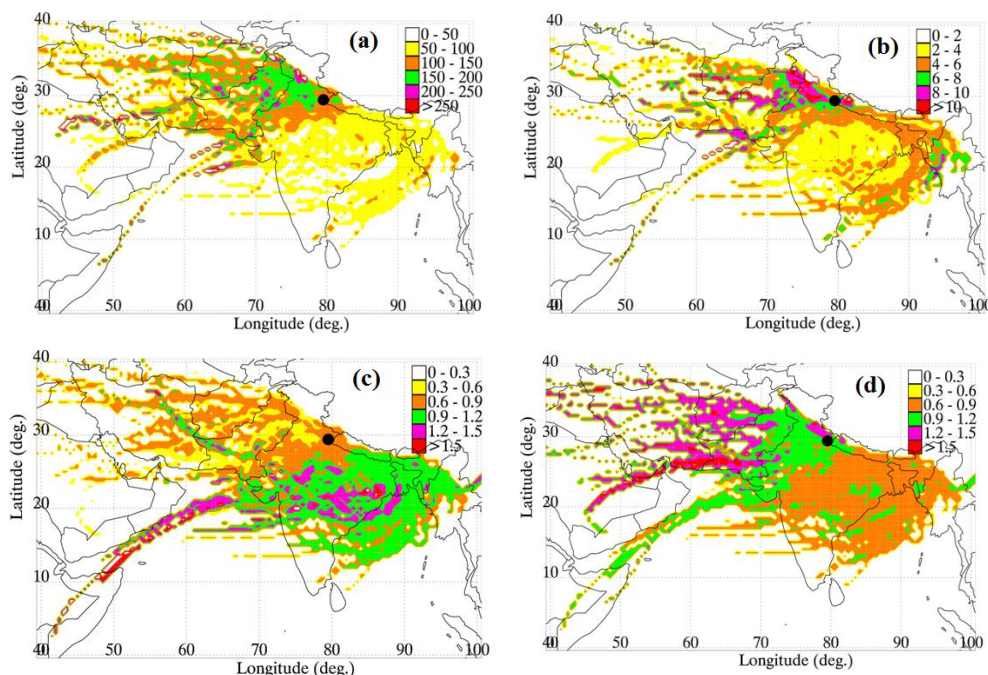


Figure 10. Concentrated weighted trajectory maps using 5-day backward trajectories ending at Nainital at 500 m for scattering (a), absorption (b) coefficients, SAE (c) and AAE (d) for $D_{10\mu\text{m}}$ particles.

(Seibert et al., 1994). The CWT analysis reveals that the major sources that contribute to the large values of σ_{sp} and σ_{ap} are detected in the northwestern and central IGP, central and southern Pakistan, arid regions in southwest Asia and, especially for σ_{ap} (Fig. 10b), eastern IGP, Bangladesh and the Bay of Bengal (BoB). It should be noted that the trajectories from eastern directions mostly occur during the monsoon, thus associated with lower σ_{sp} values (Fig. 10a) and higher SAE (Fig. 10c), while the arid regions in the west contribute to lower SAE values. Finally, the AAE plot (Fig. 10d) clearly differentiates the areas contributing to high values (southwest arid Asia) from those of moderate-to-low values (central-eastern IGP and BoB). The former regions contribute to seasonal dust and agricultural burning aerosols characterized by larger values of AAE compared to the dominance of anthropogenic and fossil-fuel burning mostly occurring in central-eastern IGP (Ram and Sarin, 2010).

Many studies (Eck et al., 2010; Russell et al., 2010; Giles et al., 2012; Vijayakumar et al., 2012, 2014) have suggested the use of correlations between the aerosol absorption and scattering properties to discriminate between different aerosol types. In this respect, we correlate the SAE with AAE for the whole set of measurements for both $D_{1\mu\text{m}}$ and $D_{10\mu\text{m}}$ groups (Fig. 11). Such a graph is able to reveal the existence of different aerosols since the wavelength dependence of scattering and absorption differentiates for the various types. As far as the scattering is concerned, the fine-mode aerosols (biomass burning, soot, urban/industrial emissions) exhibit higher values, while sea salt and desert dust

show lower values of SAE. The AAE is commonly used for aerosol characterization with values around 1 to correspond to vehicle exhausts or fossil-fuel combustions, whereas the AAE values in excess of biomass burning or dust aerosol are around 2 or even more (Kirchstetter et al., 2004; Bergstrom et al., 2007). Using AERONET retrievals, Russell et al. (2010) found AAE values varying between 1.2 and 3.0 for dust, 0.75 and 1.3 for urban/industrial and 1.2 and 2.0 for biomass burning. The range of these values seems to be significant and at the same magnitude (1.2–1.8) of those reported by Eck et al. (2010) for mixtures of dust, smoke and pollution. The current results reveal a rather well-mixed atmosphere without clear identification of specific aerosol types, as was found over pre-monsoon Kanpur (TIGERZ campaign, Giles et al., 2011). The SAE and AAE are somewhat homogeneously distributed around the mean values of SAE (0.9–1.1) and AAE (1–1.2), while few cases present large values of SAE associated with AAE of 1.0–1.5, revealing the presence of carbonaceous aerosols of mixed fossil- and biofuel combustions. The scatter plot of σ_{sp} vs. σ_{ap} (not shown) exhibited a strong correlation ($R^2 = 0.84$ for both $D_{1\mu\text{m}}$ and $D_{10\mu\text{m}}$), suggesting covariance in the scattering and absorption properties. For low aerosol loading (i.e., for σ_{sp} values below about 150 Mm^{-1}) the σ_{ap} values are almost similar to $D_{1\mu\text{m}}$ and $D_{10\mu\text{m}}$ particles, suggesting that for clean atmospheres the discrimination of the optical properties between supermicron and submicron aerosols is really difficult. Further analysis revealed a general decrease in SAE and AAE with increasing σ_{sp} , suggesting an increase in size and ageing aerosol pro-

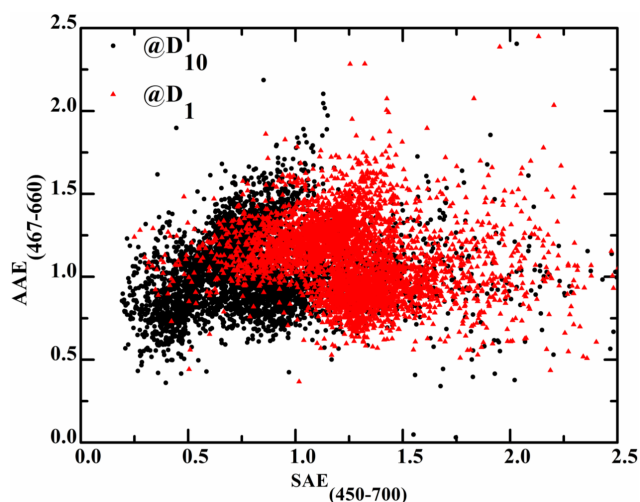


Figure 11. Correlation between scattering and absorption Ångström exponents (hourly averaged values) at Nainital for $D_{1\mu\text{m}}$ and $D_{10\mu\text{m}}$ particle-size groups.

cesses (condensation, coagulation) under more turbid atmospheres. These conditions are mostly related to LRT from northwestern IGP and southwest Asia transporting various types of aerosols via upslope flows within a deeper mixing layer.

4 Conclusions

A comprehensive analysis of several extensive and intensive properties (total scattering, backscattering, light absorption and their wavelength dependence) of near-surface aerosols was performed in the current study, aiming to investigate the temporal evolutions and influence of transported plumes and boundary-layer dynamics. The measurements via AMF were performed in Nainital, central Indian Himalayas, during June 2011–March 2012 in the framework of the GVAX campaign. More specifically, light scattering and absorption measurements made using a three-wavelength integrated nephelometer and PSAP, respectively, were analyzed along with meteorological variables, mixing-layer height and air-mass back trajectories. The main findings of the study are summarized as follows:

1. The meteorological field exhibited a seasonally changing pattern, which along with the boundary-layer dynamics and the upslope valley winds control the temporal evolution and the aerosol characteristics in Nainital. The surface wind showed a clear dominance of the northwest (winter and pre-monsoon) and southeast (summer monsoon) directions.
2. The scattering and absorption coefficients showed higher values during November and March due to the significant influence of biomass burning aerosols

and dust mixed with anthropogenic pollution, respectively, and low values during monsoon due to the rainy washout process.

3. The Ångström wavelength exponents of scattering and absorption) exhibited a seasonal variation, with a monsoon high for SAE and a late-winter-to-March high for AAE. The higher SAE values during the monsoon may be related to rainy washout and the removal of the coarser aerosol particles, while a secondary increase of SAE during winter was associated with local emissions from biofuel combustion. The latter seems to have an effect in increasing AAE values during the same period, while the higher AAE in March was associated with increased dust occurrence.
4. The particle size played a major role in the scattering coefficient and SAE, while its effect was much lesser in the absorption processes. Thus, the absorption fraction by the submicron particles ($<1\mu\text{m}$) was about 0.9 of that of $<10\mu\text{m}$ particles, while the respective scattering fraction was only 0.6.
5. The diurnal variation of both scattering and absorption coefficients revealed a noon-to-early-afternoon maximum, which was clearly defined during October to March and vanished during the monsoon period. This suggests that the largest aerosol concentrations were mostly attributed to transported plumes from the IGP and southwest Asia and not to local emissions, while the rainy washout effect modulated the diurnal cycle. Furthermore, the diurnal patterns of SAE and AAE revealed slightly higher values during early morning and evening hours due to a larger influence of the local emissions, suggesting that these aerosols are finer and more absorbing in nature than the aged transported plumes.
6. The highest values for both scattering and absorption were mostly associated with moderate winds ($3\text{--}5\text{ms}^{-1}$) and southwest air flow, suggesting a strong influence of transported aerosols from northwestern India and arid southwest Asia contributing to lower SAE values. The larger influence of the aged transported aerosol plumes controlled by the dynamics in mixing-layer height resulted in a rather well-mixed aerosol field over the site, whereas a specific aerosol type can be detected only in a few cases.

Acknowledgements. The authors gratefully acknowledge the NOAA Air Resources Laboratory for the provision of the HYSPLIT transport and dispersion model and/or READY website (<http://www.arl.noaa.gov/ready.html>) used in this publication. We are grateful to the US Department of Energy for deploying the Atmospheric Radiation Measurements Climate Research Facility and to the technical staff for providing valuable data

(<http://www.archive.arm.gov/>). This study is carried out under the GVAX (<https://www.arm.gov/sites/amf/pgh/>) project in collaboration with the DoE, IISc, SPL, ISRO and ARIES. We would like to thank the participants (scientists and technical staff) of the campaign for their valuable help and cooperation. The support of the authorities of all collaborating institutions involved in the study is acknowledged with thanks. M. K. Srivastava thanks ISRO-ARFI for the financial support. Thanks are also due to the editor and anonymous reviewers for their insightful comments and valuable suggestions, which improved the scientific content and clarity of the paper.

Edited by: X. Querol

References

- Adhikary, B., Carmichael G. R., Tang Y., Leung L. R., Qian Y., Schauer J. J., Stone E. A., Ramanathan V., and Ramana M. V.: Characterization of the seasonal cycle of south Asian aerosols: A regional-scale modeling analysis, *J. Geophys. Res.*, 112, D22S22, doi:10.1029/2006JD008143, 2007.
- Anderson, T. L. and Ogren, J. A.: Determining aerosol radiative properties using the TSI 3563 integrating Nephelometer, *Aerosol Sci. Tech.*, 29, 57–69, 1998.
- Anderson, T. L., Covert, D. S., Wheeler, J. D., Harris, J. M., Perry, K. D., Trost, B. E., Jaffe, D. J., and Ogren, J. A.: Aerosol Backscatter Fraction and Single Scattering Albedo: Measured values and uncertainties at a coastal station in the Pacific North West, *J. Geophys. Res.*, 104, 793–807, 1999.
- Andreae, T. W., Andreae, M. O., Ichoku, C., Maenhaut W., Jan, C., Karnieli, A. and Orlovsky, L.: Light scattering by dust and anthropogenic aerosol at a remote site in the Negev desert, Israel, *J. Geophys. Res.*, 107, 4008, doi:10.1029/2001JD900252, 2002.
- Andrews, E., Ogren, J. A., Bonasoni, P., Marinoni A., Cuevas E., Rodríguez S., Sun J. Y., Jaffe D. A., Fischer E. V., Baltensperger U., Weingartner E., Collaud Coen M., Sharma S., Macdonald A. M., Leaitch W. R., Lin N.-H., Laj P., Arsov T., Kalapov I., Jefferson A., and Sheridan P.: Climatology of aerosol radiative properties in the free troposphere, *Atmos. Res.*, 102, 365–393, doi:10.1016/j.atmosres.2011.08.017, 2011.
- Antón, M., Valenzuela, A., Cazorla, A., et al.: Global and diffuse shortwave irradiance during a strong desert dust episode at Granada (Spain), *Atmos. Res.*, 118, 232–239, doi:10.1016/j.atmosres.2012.07.007, 2012.
- Beegum, S., Naseema, M. K., Krishna, B. S., Suresh, S. S. K., Vinoj V., Badarinath, K. V. S., Safai, P. D., and Devara, P. C. S., Singh Sacchidanand, Vinod, Dumka U. C., Pant P.: Spatial distribution of aerosol black carbon over India during pre-monsoon Season, *Atmos. Environ.*, 43, 1071–1078, doi:10.1016/j.atmosenv.2008.11.042, 2009.
- Bergstrom, R. W., Pilewskie, P., Russell, P. B., Redemann, J., Bond, T. C., Quinn, P. K., and Sierau, B.: Spectral absorption properties of atmospheric aerosols, *Atmos. Chem. Phys.*, 7, 5937–5943, doi:10.5194/acp-7-5937-2007, 2007.
- Bollasina M. and Nigam S.: Absorbing aerosols and pre-summer monsoon hydroclimate variability over the Indian subcontinent: The challenge in investigating links, *Atmos. Res.*, 94, 338–344, doi:10.1016/j.atmosres.2009.06.008, 2009.
- Bond, T. C., Anderson, T. L., and Campbell, D.: Calibration and intercomparison of filter-based measurements of visible light absorption by aerosols, *Aerosol Sci. Tech.*, 30, 582–600, 1999.
- Bond, T. C.: Spectral dependence of visible light absorption by carbonaceous particles emitted from coal combustion, *Geophys. Res. Lett.*, 28, 4075–4078, 2001.
- Boss, E., Pegau W. S., Lee M., Twardowski M., Shybanov E., Korotaev G., and Baratange F.: Particulate backscattering ratio at LEO 15 and its use to study particle composition and distribution, *J. Geophys. Res.*, 109, C01014, doi:10.1029/2002JC001514, 2004.
- Bucci, S., Cagnazzo C., Cairo F., Di Liberto L., and Fierli, F.: Aerosol variability and atmospheric transport in the Himalayan region from CALIOP 2007–2010 observations, *Atmos. Chem. Phys.*, 14, 4369–4381, doi:10.5194/acp-14-4369-2014, 2014.
- Carrico, C. M., Kus P., Rood M. J., Quinn P. K., and Bates T. S.: Mixtures of pollution, dust, sea salt, and volcanic aerosol during ACE-Asia: Radiative properties as a function of relative humidity, *J. Geophys. Res.*, 108, 8650, doi:10.1029/2003JD003405, 2003.
- Collaud Coen, M., Weingartner, E., Schaub, D., Hueglin, C., Corrigan, C., Henning, S., Schwikowski, M., and Baltensperger, U.: Saharan dust events at the Jungfraujoch: detection by wavelength dependence of the single scattering albedo and first climatology analysis, *Atmos. Chem. Phys.*, 4, 2465–2480, doi:10.5194/acp-4-2465-2004, 2004.
- Collaud Coen, M., Weingartner, E., Furger, M., Nyeki, S., Prévôt, A. S. H., Steinbacher, M., and Baltensperger, U.: Aerosol climatology and planetary boundary influence at the Jungfraujoch analyzed by synoptic weather types, *Atmos. Chem. Phys.*, 11, 5931–5944, doi:10.5194/acp-11-5931-2011, 2011.
- Decesari, S., Facchini, M. C., Carbone, C., Giulianelli, L., Rinaldi, M., Finessi, E., Fuzzi, S., Marinoni, A., Cristofanelli, P., Duchi, R., Bonasoni, P., Vuillermoz, E., Cozic, J., Jaffrezo, J. L., and Laj, P.: Chemical composition of PM₁₀ and PM₁ at the high-altitude Himalayan station Nepal Climate Observatory-Pyramid (NCO-P) (5079 m a.s.l.), *Atmos. Chem. Phys.*, 10, 4583–4596, doi:10.5194/acp-10-4583-2010, 2010.
- Di Girolamo, L., Bond, T. C., Bramer, D., Diner, D. J., Fettingner, F., Kahn, R. A., Martonchik, J. V., Ramana, M. V., Ramanathan, V., and Rasch, P. J.: Analysis of Multi-angle Imaging Spectroradiometer (MISR) aerosol optical depths over greater India during winter 2001–2004, *Geophys. Res. Lett.*, 31, L23115, doi:10.1029/2004GL021273, 2004.
- Dipu, S., Prabha Thara V., Pandithurai G., Dudhia J., Pfister G., Rajesh K., and Goswami B. N.: Impact of elevated aerosol layer on the cloud macrophysical properties prior to monsoon onset, *Atmos. Environ.*, 70, 454–467, 2013.
- Doherty, S. J., Quinn, P. K., Jefferson, A., Carrico, C. M., Anderson, T. L., and Hegg D.: A comparison and summary of aerosol optical properties as observed in situ from aircraft, ship, and land during ACE-Asia, *J. Geophys. Res.*, 110, D04201, doi:10.1029/2004JD004964, 2005.
- Draxler, R., Stunder B., Rolph G., Stein A., and Taylor A.: HYSPLIT4 user's guide, version 4, report, NOAA, Silver Spring, Md. (available at: www.arl.noaa.gov/documents/reports/hysplit_user_guide.pdf), 2012.

- Dumka, U. C. and Kaskaoutis, D. G.: In-situ measurements of aerosol properties and estimates of radiative forcing efficiency over Gangetic–Himalayan region during the GVAX field campaign, *Atmos. Environ.*, 94, 96–105, doi:10.1016/j.atmosenv.2014.05.021, 2014.
- Dumka, U. C., Satheesh, S. K., Pant, P., Hegde, P. and Krishna Moorthy, K.: Surface changes in solar irradiance due to aerosols over central Himalayas, *Geophys. Res. Lett.*, 33, L20809, doi:10.1029/2006GL027814, 2006.
- Dumka, U. C., Krishna Moorthy, K., Satheesh, S. K., Sagar, R., and Pant, P.: Short-period modulations in aerosol optical depths over the central Himalayas: role of mesoscale processes, *J. Appl. Meteorol. Clim.*, 47, 1467–1475, doi:10.1175/2007JAMC1638.1, 2008.
- Dumka, U. C., Krishna Moorthy, K., Kumar, R., Hegde, P., Sagar, R., Pant, P., Singh, N., and Babu, S. S.: Characteristics of aerosol black carbon mass concentration over a high altitude location in the central Himalayas from multi-year measurements, *Atmos. Res.*, 96, 510–521, doi:10.1016/j.atmosres.2009.12.010, 2010.
- Dumka, U. C., Manchanda, R. K., Sinha, P. R., Sreenivasan, S., Moorthy, K. K., and Babu, S. S.: Temporal variability and radiative impact of Black Carbon aerosol over tropical urban station Hyderabad, *J. Atmos. Sol-Terr. Phys.*, 105–106, 81–90, 2013.
- Dumka, U. C., Bhattu, D., Tripathi, S. N., Kaskaoutis, D. G., and Madhavan, B. L.: Seasonal inhomogeneity in cloud precursors over Gangetic Himalayan region during GVAX campaign, *Atmos. Res.*, 155, 158–175, doi:10.1016/j.atmosres.2014.11.022, 2015.
- Eck, T. F., Holben, B. N., Sinyuk, A., Pinker, R. T., Goloub, P., Chen, H., Chatenet, B., Li, Z., Singh, R. P., Tripathi, S. N., Reid, J. S., Giles, D. M., Dubovik, O., O'Neill, N. T., Smirnov, A., Wang, P., and Xia, X.: Climatological aspects of the optical properties of fine/coarse mode aerosol mixtures, *J. Geophys. Res.*, 115, D19205, doi:10.1029/2010JD014002, 2010.
- Fierz-Schmidhauser, R., Zieger, P., Gysel, M., Kammermann, L., DeCarlo, P. F., Baltensperger, U., and Weingartner, E.: Measured and predicted aerosol light scattering enhancement factors at the high alpine site Jungfraujoch, *Atmos. Chem. Phys.*, 10, 2319–2333, doi:10.5194/acp-10-2319-2010, 2010.
- Formenti, P., Andreae, M. O., Andreae, T. W., Ichoku, C., Schebeske, G., Kettle, J., Maenhaut, W., Cafmeyer, J., Ptasinsky, J., Karnieli, A., and Lelieveld, J.: Physical and chemical characteristics of aerosols over the Negev Desert (Israel) during summer 1996, *J. Geophys. Res.*, 106, 4871–4890, 2001.
- Ganguly, D., Jayaraman, A., Rajesh, T. A., and Gadhavi, H.: Wintertime aerosol properties during foggy and non foggy days over urban center Delhi and their implications for shortwave radiative forcing, *J. Geophys. Res.*, 111, D15217, doi:10.1029/2005JD007029, 2006.
- Ganguly, D., Rasch, P. J., Wang, H., and Yoon, J. H.: Climate response of the South Asian monsoon system to anthropogenic aerosols, *J. Geophys. Res.*, 117, D13209, doi:10.1029/2012JD017508, 2012.
- Gautam, R., Hsu, N. C., Tsay, S. C., Lau, K. M., Holben, B., Bell, S., Smirnov, A., Li, C., Hansell, R., Ji, Q., Payra, S., Aryal, D., Kayastha, R., and Kim, K. M.: Accumulation of aerosols over the Indo-Gangetic plains and southern slopes of the Himalayas: distribution, properties and radiative effects during the 2009 pre-monsoon season, *Atmos. Chem. Phys.*, 11, 12841–12863, doi:10.5194/acp-11-12841-2011, 2011.
- Gautam, R., Hsu, N. C., and Lau, K.-M.: Premonsoon aerosol characterization and radiative effects over the Indo-Gangetic Plains: Implications for regional climate warming, *J. Geophys. Res.*, 115, D17208, doi:10.1029/2010JD013819, 2010.
- Giles, D. M., Holben, B. N., Tripathi, S. N., Eck, T., Newcomb, W., Slutsker, I., Dickerson, R., Thompson, A., Mattoo, S., Wang, S., Singh, R., Sinyuk, A., and Schafer, J.: Aerosol properties over the Indo–Gangetic plain: A1 mesoscale perspective from the TIGERZ experiment, *J. Geophys. Res.*, 116, D18203, doi:10.1029/2011JD015809, 2011.
- Giles, D. M., Holben, B. N., Eck, T. F., Sinyuk, A., Smirnov, A., Slutsker, I., Dickerson, R. R., Thompson, A. M., and Schafer, J. S.: An analysis of AERONET aerosol absorption properties and classifications representative of aerosol source regions, *J. Geophys. Res.*, 117, D17203, doi:10.1029/2012JD018127, 2012.
- Gopal Rama, K., Arafath, S. Md., Lingaswamy, A. P., Balakrishnaiah, G., Pavan Kumari, S., Uma Devi, K., Siva Kumar Reddy, N., Raja Obul Reddy, K., Penchal Reddy, M., Reddy, R. R., and Suresh Babu, S.: In-situ measurements of atmospheric aerosols by using Integrating Nephelometer over a semi-arid station, southern India, *Atmos. Environ.*, 86, 228–240, 2014.
- Guleria, R. P., Kuniyal, J. C., Rawat, P. S., Sharma, N. L., Thakur, H. K., Dhyani, P. P., and Singh, M.: The assessment of aerosol optical properties over Mohal in the northwestern Indian Himalayas using satellite and ground-based measurements and an influence of aerosol transport on aerosol radiative forcing, *Meteorol. Atmos. Phys.*, 113, 153–169, doi:10.1007/s00703-011-0149-5, 2011.
- Hegde, P. and Kawamura, K.: Seasonal variations of water-soluble organic carbon, dicarboxylic acids, ketocarboxylic acids, and α -dicarbonyls in Central Himalayan aerosols, *Atmos. Chem. Phys.*, 12, 6645–6665, doi:10.5194/acp-12-6645-2012, 2012.
- Hegde, P., Pant, P., Naja, M., Dumka, U. C., and Sagar, R.: South Asian dust episode in June 2006: aerosol observations in the central Himalayas, *Geophys. Res. Lett.*, 34, L23802, doi:10.1029/2007GL030692, 2007.
- Heintzenberg, J., Wiedensohler, A., Tuch, T. M., Covert, D. S., Sheridan, P., Ogren, J. A., Gras, J., Nessler, R., Kleefeld, C., Kalivitis, N., Aaltonen, V., Wilhelm, R. T., and Havlicek, M.: Intercomparison and aerosol calibrations of 12 commercial integrating Nephelometer of three manufacturers, *J. Atmos. Ocean. Tech.*, 23, 902–914, 2006.
- Hyvärinen, A.-P., Raatikainen, T., Brus, D., Komppula, M., Panwar, T. S., Hooda, R. K., Sharma, V. P., and Lihavainen, H.: Effect of the summer monsoon on aerosols at two measurement stations in Northern India – Part 1: PM and BC concentrations, *Atmos. Chem. Phys.*, 11, 8271–8282, doi:10.5194/acp-11-8271-2011, 2011a.
- Hyvärinen, A.-P., Raatikainen, T., Komppula, M., Mielonen, T., Sundström, A.-M., Brus, D., Panwar, T. S., Hooda, R. K., Sharma, V. P., de Leeuw, G., and Lihavainen, H.: Effect of the summer monsoon on aerosols at two measurement stations in Northern India – Part 2: Physical and optical properties, *Atmos. Chem. Phys.*, 11, 8283–8294, doi:10.5194/acp-11-8283-2011, 2011b.

- Hyvärinen, A.-P., Lihavainen, H., Komppula, M., Sharma, V. P., Kerminen, V.-M., Panwar, T. S., and Viisanen, Y.: Continuous measurements of optical properties of atmospheric aerosols in Mukteshwar, Northern India, *J. Geophys. Res.*, 114, D08207, doi:10.1029/2008JD011489, 2009.
- Jayaraman, A., Gadhavi, H., Misra, A., Ganguly, D., Ramachandran, S., and Rajesh, T. A.: Spatial variations in aerosol characteristics and regional radiative forcing over India: measurements and modeling of 2004 road campaign experiment, *Atmos. Environ.*, 40, 6504–6515, doi:10.1016/j.atmosenv.2006.01.034, 2006.
- Jefferson, A.: Aerosol Observing System (AOS) Handbook, DOE/SC-ARM/TR-014, (http://www.arm.gov/publications/tech_reports/handbooks/aos_handbook.pdf), 2011.
- Kaskaoutis, D. G., Singh, R. P., Gautam, R., Sharma, M., Kosmopoulos, P. G., and Tripathi, S. N.: Variability and trends of aerosol properties over Kanpur, northern India using AERONET data (2001–10), *Environ. Res. Lett.*, 7, 024003, doi:10.1088/1748-9326/7/2/024003, 2012.
- Kaskaoutis, D. G., Sinha, P. R., Vinoj, V., Kosmopoulos, P. G., Tripathi, S. N., Misra, A., Sharma, M., and Singh, R. P.: Aerosol properties and radiative forcing over Kanpur during severe aerosol loading conditions, *Atmos. Environ.*, 79, 7–19, doi:10.1016/j.atmosenv.2013.06.020, 2013.
- Kaskaoutis, D. G., Kumar, S., Sharma, D., Singh, R. P., Kharol, S. K., Sharma, M., Singh, A. K., Singh, S., Singh, A., and Singh, D.: Effects of crop residue burning on aerosol properties, plume characteristics and longrange transport over northern India, *J. Geophys. Res.*, 119, 5424–5444, doi:10.1002/2013JD021357, 2014.
- Kirchstetter, T. W., Novakov, T., and Hobbs, P. V.: Evidence that the spectral dependence of light absorption by aerosols is affected by organic carbon, *J. Geophys. Res.*, 109, D21208, doi:10.1029/2004JD004999, 2004.
- Komppula, M., Lihavainen, H., Hyvärinen, A.-P., Kerminen, V.-M., Panwar, T. S., Sharma, V. P., and Viisanen, Y.: Physical properties of aerosol particles at a Himalayan background site in India, *J. Geophys. Res.*, 114, D12202, doi:10.1029/2008JD011007, 2009.
- Kopacz, M., Jacob, D. J., Fisher, J. A., Logan, J. A., Zhang, L., Megretskaya, I. A., Yantosca, R. M., Singh, K., Henze, D. K., Burrows, J. P., Buchwitz, M., Khlystova, I., McMillan, W. W., Gille, J. C., Edwards, D. P., Eldering, A., Thouret, V., and Nedelec, P.: Global estimates of CO sources with high resolution by adjoint inversion of multiple satellite datasets (MOPITT, AIRS, SCIAMACHY, TES), *Atmos. Chem. Phys.*, 10, 855–876, doi:10.5194/acp-10-855-2010, 2010.
- Kotamarthi, V. R. and Satheesh, S. K.: Ganges Valley Aerosol Experiment, Air & Waste Management Association, Em, The magazine for environmental managers, 2011.
- Kumar, R., Barth, M. C., Pfister, G. G., Naja, M., and Brasseur, G. P.: WRF-Chem simulations of a typical pre-monsoon dust storm in northern India: influences on aerosol optical properties and radiation budget, *Atmos. Chem. Phys.*, 14, 2431–2446, doi:10.5194/acp-14-2431-2014, 2014.
- Lau, K. M., Kim, M. K., and Kim, K. M.: Asian summer monsoon anomalies induced by aerosol direct forcing: the role of the Tibetan Plateau, *Clim. Dynam.*, 26, 855–864, doi:10.1007/s00382-014-2055-2, 2006.
- Lawrence, M. G. and Lelieveld, J.: Atmospheric pollutant outflow from Southern Asia: a review, *Atmos. Chem. Phys.*, 10, 11017–11096, doi:10.5194/acp-10-11017-2010, 2010.
- León, J.-F. and Legrand, M.: Mineral dust sources in the surroundings of the north Indian Ocean, *Geophys. Res. Lett.*, 30, 1309, doi:10.1029/2002GL016690, 2003.
- Liu, Z., Liu, D., Huang, J., Vaughan, M., Uno, I., Sugimoto, N., Kitaka, C., Trepte, C., Wang, Z., Hostetler, C., and Winker, D.: Airborne dust distributions over the Tibetan Plateau and surrounding areas derived from the first year of CALIPSO lidar observations, *Atmos. Chem. Phys.*, 8, 5045–5060, doi:10.5194/acp-8-5045-2008, 2008.
- Lu, Z., Zhang, Q., and Streets, D. G.: Sulfur dioxide and primary carbonaceous aerosol emissions in China and India, 1996–2010, *Atmos. Chem. Phys.*, 11, 9839–9864, doi:10.5194/acp-11-9839-2011, 2011.
- Manoharan, V. S., Kotamarthi, R., Feng, Y., and Cadeddu, M. P.: Increased absorption by coarse aerosol particles over the Gangetic–Himalayan region, *Atmos. Chem. Phys.*, 14, 1159–1165, doi:10.5194/acp-14-1159-2014, 2014.
- Manoj, M. G., Devara, P. C. S., Safai, P. D., and Goswami, B. N.: Absorbing aerosols facilitate transition of Indian monsoon breaks to active spells, *Clim. Dynam.*, 37, 2181–2198, 2011.
- Marcq, S., Laj, P., Roger, J. C., Villani, P., Sellegri, K., Bonasoni, P., Marinoni, A., Cristofanelli, P., Verza, G. P., and Bergin, M.: Aerosol optical properties and radiative forcing in the high Himalaya based on measurements at the Nepal Climate Observatory-Pyramid site (5079 m a.s.l.), *Atmos. Chem. Phys.*, 10, 5859–5872, doi:10.5194/acp-10-5859-2010, 2010.
- Marinoni, A., Cristofanelli, P., Laj, P., Duchi, R., Calzolari, F., Decesari, S., Sellegri, K., Vuillermoz, E., Verza, G. P., Villani, P., and Bonasoni, P.: Aerosol mass and black carbon concentrations, a two year record at NCO-P (5079 m, Southern Himalayas), *Atmos. Chem. Phys.*, 10, 8551–8562, doi:10.5194/acp-10-8551-2010, 2010.
- Nakajima, T., Yoon, S.-C., Ramanathan, V., Shi, G.-Y., Takemura, T., Higurashi, A., Takamura, T., Aoki, K., Sohn, B.-J., Kim, S.-W., Tsuruta, H., Sugimoto, N., Shimizu, A., Tanimoto, H., Sawa, Y., Lin, N.-H., Lee, C.-T., Goto, D., and Schutgens, N.: Overview of the atmospheric Brown Cloud East Asian Regional Experiment 2005 and a study of the aerosol direct radiative forcing in east Asia, *J. Geophys. Res.*, 112, D24S91, doi:10.1029/2007JD009009, 2007.
- Neitola, K., Asmi, E., Komppula, M., Hyvärinen, A.-P., Raatikainen, T., Panwar, T. S., Sharma, V. P. and Lihavainen, H.: New particle formation infrequently observed in Himalayan foothills – why?, *Atmos. Chem. Phys.*, 11, 8447–8458, doi:10.5194/acp-11-8447-2011, 2011.
- Ogren, J. A.: Comment on “Calibration and Intercomparison of Filter-Based Measurements of Visible Light Absorption by Aerosols”, *Aerosol Sci. Tech.*, 44, 589–591, 2010.
- Pandolfi, M., Ripoll, A., Querol, X., and Alastuey, A.: Climatology of aerosol optical properties and black carbon mass absorption cross section at a remote high-altitude site in the western Mediterranean Basin, *Atmos. Chem. Phys.*, 14, 6443–6460, doi:10.5194/acp-14-6443-2014, 2014.
- Pant, P., Hegde, P., Dumka, U. C., Sagar, R., Satheesh, S. K., Moorthy, K. K., Saha, A., and Srivastava, M. K.: Aerosol characteristics at a high-altitude location in central Himalayas: Optical

- properties and radiative forcing, *J. Geophys. Res.*, 111, D17206, doi:10.1029/2005JD006768, 2006.
- Panwar, T. S., Hooda Rakesh, K., Lihavainen, H., Hyvärinen, A. P., Sharma, V. P., and Viisanen, Y.: Atmospheric aerosols at a regional background Himalayan site-Mukteshwar, India, *Environ. Monit. Assess.*, 185, 4753–4764, doi:10.1007/s10661-012-2902-8, 2013.
- Pathak, B., Bhuyan, P. K., Biswas, J., and Takemura, T.: Long term climatology of Particulate Matter and associated microphysical and optical properties over Dibrugarh, North-East India and inter-comparison with SPRINTARS simulations, *Atmos. Environ.*, 69, 334–344, 2013.
- Prabha T. V., Karipot, A., Axisa D., Padmakumari B., Maheskumar R. S., Konwar M., Kulkarni J. R., and Goswami B. N.: Scale interactions near the foothills of Himalaya during CAIPEEX, *J. Geophys. Res.*, 117, D10203, doi:10.1029/2011JD0167, 2012.
- Raatikainen T., Hyvärinen A.-P., Hatakka J., Panwar T. S., Hooda R. K., Sharma, V. P., and Lihavainen, H.: The effect of boundary layer dynamics on aerosol properties at the Indo-Gangetic plains and at the foothills of the Himalayas, *Atmos. Environ.*, 89, 548–555, doi:10.1016/j.atmosenv.2014.02.058, 2014.
- Ram, K. and Sarin, M. M.: Spatio-temporal variability in atmospheric abundances of EC, OC and WSOC over Northern India, *J. Aerosol Sci.*, 41, 88–98, doi:10.1016/j.jaerosci.2009.11.004, 2010.
- Ram, K., Sarin, M. M., and Hedge, P.: Atmospheric abundances of primary and secondary carbonaceous species at two high-altitude sites in India: sources and temporal variability, *Atmos. Environ.*, 42, 6785–6796, 2008.
- Ram, K., Sarin, M. M., and Hegde, P.: Long-term record of aerosol optical properties and chemical composition from a high-altitude site (Manora Peak) in Central Himalaya, *Atmos. Chem. Phys.*, 10, 11791–11803, doi:10.5194/acp-10-11791-2010, 2010.
- Ramanathan, V., Chung, C., Kim, D., Bettge, T., Buja, L., Kiehl, J. T., Washington, W. M., Fu, Q., Sikka, D. R., and Wild, M.: Atmospheric brown clouds: impacts on South Asian climate and hydrological cycle, *P. Natl. Acad. Sci. USA*, 102, 5326–5333, doi:10.1073/pnas.0500656102, 2005.
- Ramanathan, V., Li, F., Ramana, M. V., Praveen, P. S., Kim, D., Corrigan, C. E., Nguyen, H., Stone, E. A., Schauer, J. J., Carmichael, G. R., Adhikary, B., and Yoon, S. C.: Atmospheric brown clouds: Hemispherical and regional variations in long-range transport, absorption, and radiative forcing, *J. Geophys. Res.*, 112, D22S21, doi:10.1029/2006JD008124, 2007.
- Randles, C. A. and Ramaswamy, V.: Absorbing aerosols over Asia: a geophysical fluid dynamics laboratory general circulation model sensitivity study of model response to aerosol optical depth and aerosol absorption, *J. Geophys. Res.*, 113, D21203, doi:10.1029/2008JD010140, 2008.
- Russell, P. B., Bergstrom, R. W., Shinozuka, Y., Clarke, A. D., DeCarlo, P. F., Jimenez, J. L., Livingston, J. M., Redemann, J., Dubovik, O., and Strawa, A.: Absorption Angstrom Exponent in AERONET and related data as an indicator of aerosol composition, *Atmos. Chem. Phys.*, 10, 1155–1169, doi:10.5194/acp-10-1155-2010, 2010.
- Sarkar, C., Chatterjee, A., Singh, A.K., Ghosh, S.K., and Raha, S.: Characterization of Black Carbon aerosols over Darjeeling – A high altitude Himalayan station in Eastern India, *Aeros. Air Qual. Res.*, in press, doi:10.4209/aaqr.2014.02.0028, 2014.
- Seibert, P., Kromp-Kolb, H., Baltensperger, U., Jost, D. T., Schwikowski, M., Kasper, A. and Puxbaum, H.: Trajectory analysis of aerosol measurements at high alpine sites, in: *Transport and Transformation of Pollutants in the Troposphere: Proceedings of EUROTRAC Symposium '94*, edited by: Borrell, P. M., Cvitas, T., and Seiler, W., 689–693, SPB Acad. Publ., Hague, The Netherlands, 1994.
- Sheridan, P. J. and Ogren, J. A.: Observations of the vertical and regional variability of aerosol optical properties over central and eastern North America, *J. Geophys. Res.*, 104, 16793–16805, doi:10.1029/1999JD900241, 1999.
- Sheridan, P. J., Delene, D. J., and Ogren, J. A.: Four years of continuous surface aerosol measurements from the Department of Energy's Atmospheric Radiation Measurement Program Southern Great Plains Cloud and Radiation Testbed site, *J. Geophys. Res.*, 106, 20735–20747, doi:10.1029/2001JD000785, 2001.
- Srivastava, A. K., Singh, S., Pant, P., and Dumka, U. C.: Characteristics of Black Carbon over Delhi and Manora Peak – a comparative study, *Atmos. Sci. Lett.* 13, 223–230, 2012.
- Titos, G., Jefferson, A., Sheridan, P. J., Andrews, E., Lyamani, H., Alados-Arboledas L., and Ogren J. A.: Aerosol light-scattering enhancement due to water uptake during TCAP campaign, *Atmos. Chem. Phys.*, 14, 7031–7043, doi:10.5194/acp-14-7031-2014, 2014a.
- Titos, G., Lyamani, H., Cazorla, A., Sorribas, M., Foyo-Moreno, I., Wiedensohler, A., and Alados-Arboledas, L.: Study of the relative humidity dependence of aerosol light-scattering in southern Spain, *Tellus B*, 66, 24536, <http://dx.doi.org/10.3402/tellusb.v66.24536>, 2014b.
- Twardowski, M. S., Boss, E., Macdonald, J. B., Scott Pegau, W., Barnard, A. H., and Zaneveld, J. R. V.: A model for estimating bulk refractive index from the optical backscattering ratio and the implications for understanding particle composition in case I and case II waters, *J. Geophys. Res.*, 106, 14129–14142, 2001.
- Vijayakumar, K., Devara, P. C. S., and Sonbawne, S. M.: Type-segregated aerosol effects on regional monsoon activity: A study using ground-based experiments and model simulations, *Atmos. Environ.*, 99, 650–659, 2014.
- Vijayakumar, K., Devara, P. C. S., and Simha, C. P.: Aerosol features during drought and normal monsoon years: A study undertaken with multi-platform measurements over a tropical urban site, *Aero. Air Qual. Res.*, 12, 1444–1458, 2012.
- Virkkula A., Backman J., Aalto P. P., Hulkkonen M., Riuttanen L., Nieminen T., dal Maso M., Sogacheva L., de Leeuw G., and Kulmala M.: Seasonal cycle, size dependencies, and source analyses of aerosol optical properties at the SMEAR II measurement station in Hyytiälä, Finland, *Atmos. Chem. Phys.*, 11, 4445–4468, doi:10.5194/acp-11-4445-2011, 2011.
- Xu, C., Ma Y. M., Pandey A., Cong Z. Y., Yang K., Zhu Z. K., Wang J. M., Amaty P. M., and Zhao L: Similarities and differences of aerosol optical properties between southern and northern slopes of the Himalayas, *Atmos. Chem. Phys.*, 14, 3133–3149, doi:10.5194/acp-14-3133-2014, 2014.